Catena 222 (2023) 106853

Contents lists available at ScienceDirect

Catena

journal homepage: www.elsevier.com/locate/catena

Effects of roots cohesion on regional distributed slope stability modelling

Elena Benedetta Masi [a,*], Veronica Tofani [a], Guglielmo Rossi [b], Sabatino Cuomo [c], Wei Wu [d], Diana Salciarini [e], Enrica Caporali [f], Filippo Catani [a,g]

[a] Department of Earth Sciences, University of Florence, Via La Pira, 4, Florence, 50121, Italy
[b] Civil Protection Centre, University of Florence, Largo Enrico Fermi, 2, Florence, 50125, Italy
[c] Department of Civil Engineering, University of Salerno, Via Giovanni Paolo II, 132, Fisciano (SA) 84084, Italy
[d] Institut für Geotechnik, Universität für Bodenkultur, Feistmantelstraße, 4, Wien, 1180, Austria
[e] Department of Civil and Environmental Engineering, University of Perugia, Via G. Duranti, Perugia, 06125, Italy
[f] Department of Civil and Environmental Engineering, University of Florence, Via di S. Marta, 3, Florence, 50139, Italy
[g] Department of Geosciences, University of Padova, Via Giovanni Gradenigo, 6, Padova, 35131, Italy

ARTICLE INFO

Keywords:
Shallow landslides
Root reinforcement
Slope stability modelling
Regional landslides forecasting

ABSTRACT

We present a regionally distributed slope stability modelling for shallow landslides considering the effect of plant roots. Our modelling is based on the physically-based distributed slope stability model, HIRESSS (HIgh REsolution Slope Stability Simulator). Thanks to the parallel structure, our code is well suited to perform fast assessment of slope stability over large spatial and temporal scales. The reinforcing effect of plant roots is implemented into the code by considering the local plant species and their spatial variations. The probabilistic nature of the stability of slopes is considered by performing Monte Carlo simulations. Our model is applied to two study areas in Italy. The numerical results are compared with the collected data from these areas. The model predictions show that the effect of plant root is sensitive to rainfall intensity and duration. Our model prediction shows only minor influence of plant root on slope stability particularly for the soil conditions near saturation.

1. Introduction

The study and modelling of the shallow landslides require constant efforts from research for two main reasons. First, shallow landslides are often pre-cursors of impending major debris flow. They commonly start as shallow mass movements involving only some tens of cubic meters of terrain at the beginning but can commonly evolve into rapid mass movements assuming characteristics of debris avalanches and flows. The second aspect is that these landslides are predominantly triggered by intense rainfall. As such, rarely single failures happen, rather, multiple and diffused landslide events are often triggered in the region hit by the rainfall. Some of the catastrophic regional landslide events consisted of clusters of debris avalanches and debris flows triggered by heavy rainfall. The site conditions favorable to trigger shallow landslides may vary in a wide spectrum depending on the soil conditions, morphology, vegetation cover and land use.

Due to the abundance of areas susceptible to shallow landslides, the scientific community relies mainly on two approaches to provide support to the administrations and civil protection agencies in the mitigation of the risk: the hazard assessment in support of the land management and the forecasting of temporal and spatial distribution of the events for early warning systems. The forecasting of shallow landslides adopts approaches known as empirical or uses physically-based slope stability models. The first model category is based on statistic consideration by searching functional relations between the triggering factors (as the rainfall intensity/duration) and the actual events occurred in a specific area to define warning thresholds. To the second category belong the physics-based approaches that combine hydrological models and slope stability analyses to predict hazard areas. Commonly, the stability model is based on the infinite slope model. The soil moisture dynamics is generally based on a modified version of the steady-state wetness index (Montgomery and Dietrich 1994; Pack et al. 1998; Borga et al. 2002; Arnone et al. 2011) or an approximation of the Richards equation (Iverson 2000; Baum et al., 2002; Simoni et al. 2008). Such models provide slope stability evaluations based on the Factor of Safety (FS) (e.g., Pack et al. 1998;(Baum et al., 2002)) or as a function of the transmissivity (seepage flow) and rainfall rate (e.g., Montgomery and Dietrich 1994; Borga et al. 2002).

Nowadays the slope stability models have been further developed to include the effect of plants, since the beneficial effect of vegetation in the

* Corresponding author.
E-mail address: elenabenedetta.masi@unifi.it (E.B. Masi).

https://doi.org/10.1016/j.catena.2022.106853
Received 1 July 2022; Received in revised form 23 November 2022; Accepted 2 December 2022
Available online 15 December 2022

stability of slopes is widely recognized. Vegetation is known to reduce the failure susceptibility to rainfall triggered shallow landslides through different mechanical and hydrological pathways. One of the main mechanical effects is the reinforcement of soil by plant roots in which gives rise to an increase of the soil shear strength.

The spatial variability that characterizes the root reinforcement makes it a challenging task to integrate the root reinforcement into the slope stability models, especially when large areas are considered. Many approaches to estimate the root reinforcement in large areas have been proposed, e.g. by extrapolating an average or uniform distribution of point measurements to estimate cohesion (Montgomery and Dietrich, 1994; Pack et al., 1998); by using size, geometry and distribution of the plants to estimate local minima in root strength (Roering et al., 2003; Sakals and Sidle, 2004; (Cislaghi et al., 2017a); Temgoua et al., 2017); by relating remotely sensed metrics of vegetation to the root reinforcement (Chiang and Chang, 2011; Hwang et al., 2015); and by applying eco-hydrologic models to estimate the reinforcement at slope or regional scale (Preti et al., 2010; Lepore et al., 2013; Tron et al., 2014, Arnone et al., 2016). Hales (2018) developed a model to estimate the root reinforcement of extensive areas, deriving the root densities from a global wood density database. Other authors (Salvatici et al., 2018 and (Cuomo et al., 2021) approached instead to the problem taking advantage of Monte Carlo simulations to stochastically reproduce the natural variability of the root reinforcement.

A perusal of the above publications shows that the following two aspects deserve our attention when applying distributed slope stability models to vegetated slopes. First, the root reinforcement in the models should reflect the spatial and temporal scales. Moreover, the local plant species, as well as their spatial variation should be considered and validated at regional scale. Second, the distributed model should be robust and efficient to provide fast landslide forecasting. Our paper is poised to cater to these needs.

Considering the importance of regional forecasting of rainfall triggered shallow landslides, the relevant role of vegetation in the slope stability and the mentioned needs in this field, the purposes of the present research are i) modifying a distributed slope stability model capable of supporting quick assessment of slope stability at a regional scale to consider the root reinforcement patterns in regional slope stability analysis; ii) individuating an efficient approach to estimate the root reinforcement at regional scale, favoring applicable methods using already available territorial information or derivable in reasonable time; iii) evaluating the effect of the integration of the root reinforcement on the results of regional slope stability simulations of long periods, to make an evaluation of the approach adopted to estimate the root reinforcement in wide areas, and to assess the eventual improvements obtained in the forecasting capabilities of the distributed slope stability model.

2. Materials and methods

The HIRESSS model (Rossi et al., 2013) was chosen to perform the slope stability analysis because of its features such as i) the capability of computing the factor of safety at each time step and not only at the end of the rainfall event; ii) the variable-depth computation of slope stability; iii) the taking into account of the contribution of soil suction in unsaturated conditions; iv) the probabilistic treatment of the uncertainties in the main hydrological and mechanical parameters and, thus, of the factor of safety; v) high processing speed even for extensive area analysis. HIRESSS is based on a physical model composed of a hydrological module and a geotechnical module. The hydrological model receives the rainfall data as dynamical input and provides the pressure head as a perturbation to the geotechnical model, that provides results in terms of failure probabilities. The structure of the software is inspired by the work of Iverson (Iverson, 2000) also used in the TRIGRS software. The hydrological model is based on an analytical solution of an approximated form of Richards equation under the wet condition hypothesis, and it is introduced as a modelled form of hydraulic diffusivity. The geotechnical model is based on an infinite slope model that considers the unsaturated conditions. During the stability analysis, the proposed model considers the increase in strength and cohesion due to matric suction in unsaturated soil due to negative pressure head. Moreover, the soil mass variation on partially saturated soil caused by the water infiltration is modelled. The model then provides for Monte Carlo simulations to manage the typical geotechnical parameters incertitude. The Monte Carlo simulation manages a probability distribution of the input parameter, and the ending results of the simulator are slope failure probabilities. Applications of HIRESSS in different geological-geomorphological contexts and soil typologies have been presented in Rossi et al., 2013; Tofani et al. 2017; Salvatici et al., 2018; (Cuomo et al., 2021).

One of the main scopes of this study was identify an efficient method to consider the effect of the root reinforcement on slope stability at a regional scale, to integrate the parameter in HIRESSS and testing consequent possible improvements of its forecasting capabilities.

Considering approaches already explored described by the scientific community, advantages, and drawbacks of either procedure and the characteristics of HIRESSS, we individuated the following approach to evaluate the root reinforcement at a regional scale, consisting in:

i. identifying the plant species of the study area and determining their distribution from in-situ observations and already existing vegetational maps;
ii. assigning root cohesion mean value and variation range to each subarea according to its dominant plant species and root cohesion values reported in literature;
iii. reproducing the natural spatial variability of the parameter through Monte Carlo simulations.

Root tensile strength of plant species has been widely studied through in-situ and laboratory tests (among others Genet et al., 2011;; Hales et al., 2013; Anderson et al., 1989; Schmidt et al., 2001; Bischetti et al., 2009; Norris, 2005; Burylo et al., 2011; Tosi, 2007). But the estimate of root cohesion values also needs the knowledge of root profiles (root densities at different depth), so that root cohesion values are not equally abundant in literature. Some recent works have been focusing on the root reinforcement exerted by a high-value plantation cultivated in steep hills often affected by landslides, the vineyards: Bordoni et al. (2016), (Cislaghi et al., 2017b), and Bordoni et al. (2020). Authors as Wang et al. (2019), Chiaradia et al. (2016), Likitlersuang et al. (2017), Gonzalez-Oullari and Mickowski (2017) have studied the hydrological and mechanical root reinforcement of other cultivated species and many spontaneous plant species.

The Monte Carlo simulations are made by HIRESSS, which treats every geotechnical and hydrological input data through Monte Carlo simulations to manage the intrinsic uncertainty of these parameters.

HIRESSS had been modified to consider the effect of the root reinforcement to the stability of slopes. The root reinforcement was modelled as a component of the total cohesion of soil (e.g., Waldron and Dakessian, 1981; Gray and Ohashi, 1983; Operstein and Frydaman, 2000; Giadrossich et al., 2010). Original FS (factor of safety) equations (Rossi et al., 2013) were modified considering the root reinforcement (c_r) as follows:

$$c_{tot} = c' + c_r \tag{1}$$

where c_{tot} is the total cohesion of the soil; c' is the "standard cohesion", the component of cohesion commonly measured with laboratory test as the direct shear test. In accordance with one of the first developed and most adopted model (Wu et al.,1979), the root reinforcement (or root cohesion) can be considered equal to:

$$c_r = kt_r \tag{2}$$

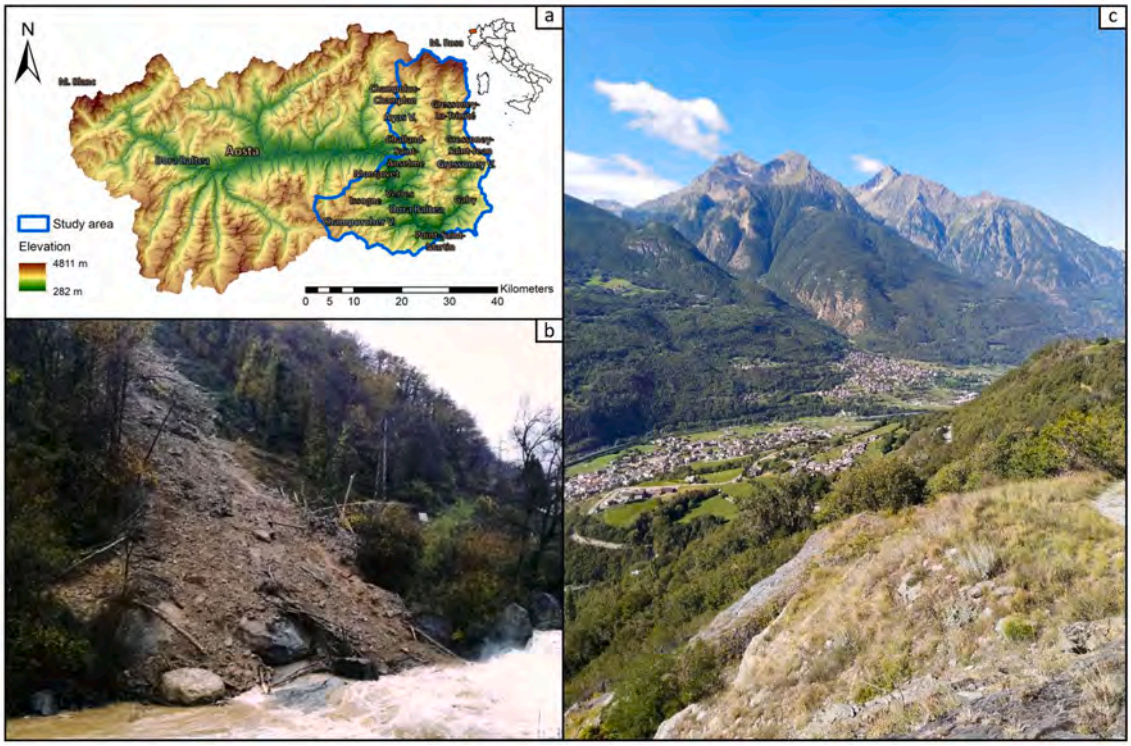

Fig. 1. a) Valle d'Aosta region, northwest Italy, evidenced in blue the study area "Alert zone B"; b) Debris flow triggered during a rainfall event in 2019 in Fontainemore municipality, Valle d'Aosta (photo courtesy of Centro Funzionale Regione Autonoma Valle d'Aosta); c) View of a main valley bottom and surrounding reliefs of the study area. (For interpretation of the references to color in this figure legend, the reader is referred to the web version of this article.)

$$t_r = \sum_{n=1}^{N} t_{r,n} RAR_n \quad (3)$$

where t_r is the root failure strength (tensile, frictional, or compressive) of roots per unit area of soil, k is a coefficient dependent on the effective soil friction angle and the orientation of roots, N are the classes of roots grouped for diameter, $t_{r,n}$ is the average tensile strength of roots of class n, RAR_n is the root area ratio (proportion of area occupied by roots per unit area of soil) of the class n. This model tends to overestimate the root reinforcement essentially due to the assumption that all tensile strength of the roots is mobilized during the soil shearing, and that all roots break simultaneously (Waldron and Dakessian, 1981, Greenway, 1987, Pollen et al., 2004, De Baets et al., 2008). In order to limit this overestimation of

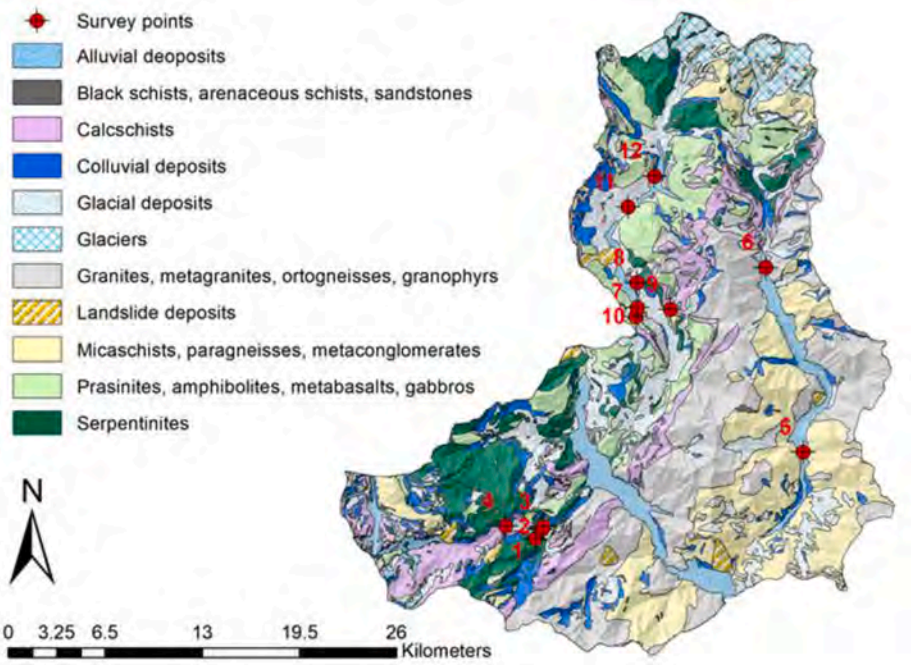

Fig. 2. Spatial distribution of survey points and geological map of the Valle d'Aosta case study.

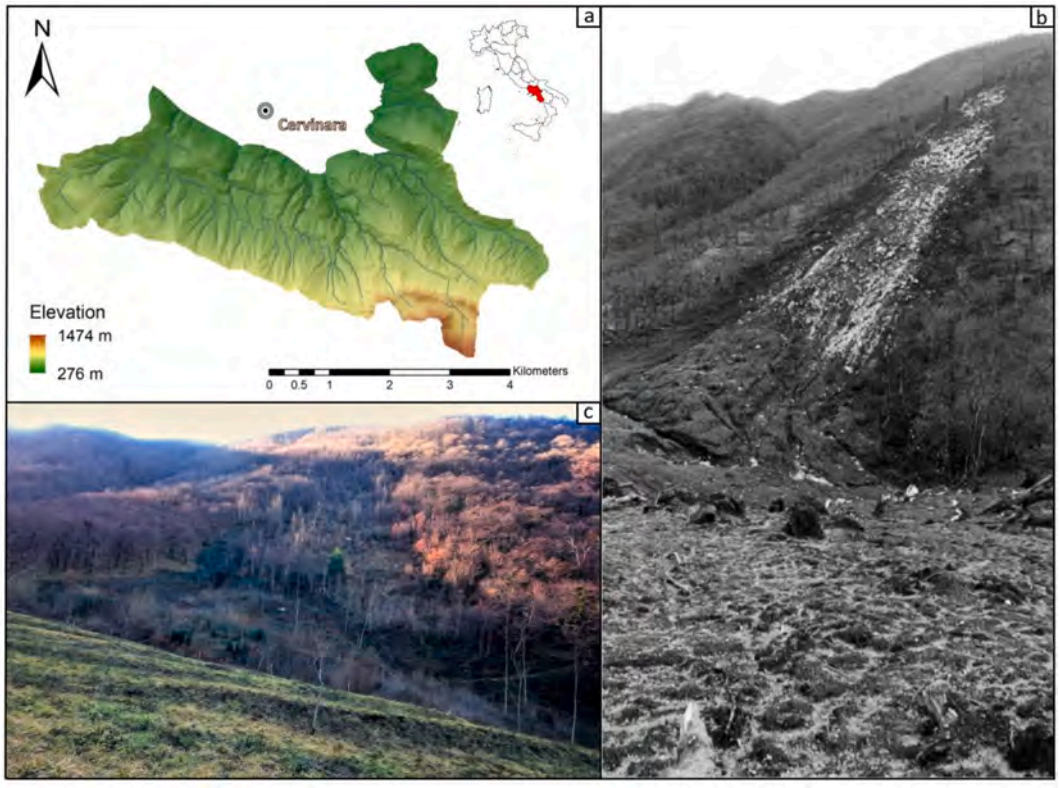

Fig. 3. A) the study area in the Cervinara (AV) municipality, Campania Region, southwest Italy; b) One of the landslides triggered during the December 1999 event (Fiorillo et al., 2001); c) Same landslide captured in January 2019.

the root reinforcement, Pollen and Simon (2005) and Pollen (2007) presented a model based on the principles of the rupture of fiber bundle (FBM), the RipRoot, in which the progressive breaking of roots is considered:

$$t_r = \max(t_{r,j} RAR_j j) \quad (4)$$

where (with roots ordered from the strongest to the weakest (1 to N) j is the weakest root that is still intact upon loading of the root bundle of N roots, RAR_j is the RAR of the root j and $t_{r,j}$ is the strength of the weakest intact root.

For our study, we found root cohesion values about the dominant plant species of the study areas in Bischetti et al., 2009, Burylo et al., 2011, Norris, 2005. In the case of some plant species, it was not possible to refer to literature works specifically dedicated to them and we have relied on Hales, 2018 considering biome-level root cohesion values. Root cohesion values based on FBM were adopted as they are, as well as values based on Wu model about herbaceous plant species, in the case of values based on Wu model about shrubs and trees species we have applied a reduction factor of 0.50 for accounting for the well-known overestimation due to the use of Wu models to estimate the root reinforcement (Waldron and Dakessian, 1981; Pollen and Simon, 2005; Wu, 2013; Arnone et al., 2016, Preti and Schwarz, 2006, Schwarz et al., 2010; Zydron and Skorski, 2018).

The modified version of HIRESSS equation for factor of safety (FS) at unsaturated conditions including the root reinforcement effect is as follows:

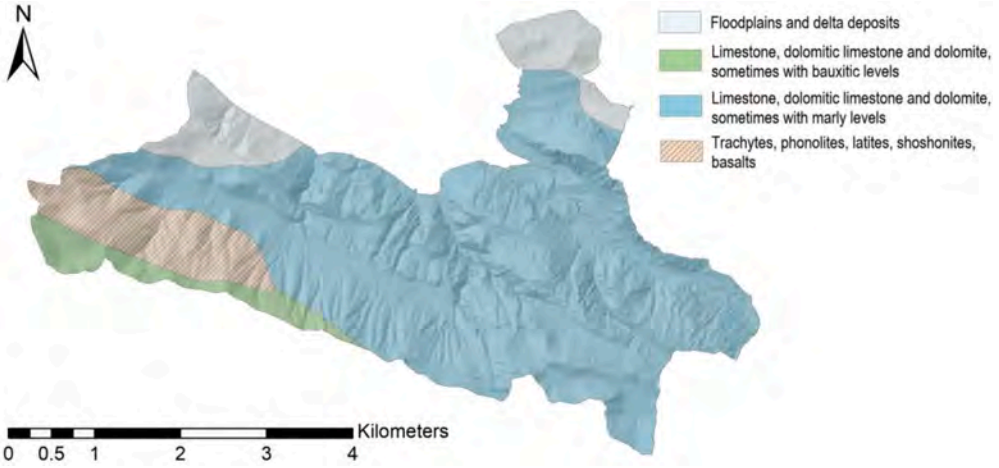

Fig. 4. Geolithological map of the Cervinara study area.

$$FS = \frac{\tan\varphi}{\tan\alpha} + \frac{c_{tot}}{\gamma_d y \sin\alpha} + \frac{\gamma_w h \tan(\varphi)\left(\frac{1}{\left[1+\left(h_b^{-1}|h|\right)^{(\lambda-1)}\right]^{\left(\frac{\lambda}{\lambda+1}\right)}}\right)}{\gamma_d y sin\alpha} \quad (5)$$

where φ *is* the friction angle, α the slope angle, γ_d the dry soil unit weight, y the depth of the column of soil, γ_w the water unit weight, h the pressure head, h_b is the bubbling pressure and λ the pore size index distribution.

In the saturated conditions, the equation for FS becomes:

$$FS = \frac{\tan\varphi}{\tan\alpha} + \frac{c_{tot}}{[\gamma_d(y-h)+\gamma_s h]\sin\alpha} - \frac{\gamma_w h \tan(\varphi)}{[\gamma_d(y-h)+\gamma_s h] sin\alpha} \quad (6)$$

whvere γ_s is the saturated soil unit weight.

2.1. Study areas

The study areas are represented by i) the eastern part of the Valle D'Aosta (northern Italy) with an extension of about 837 km^2, named "Alert zone B" by the regional civil protection authorities (Fig. 1 and Fig. 2) and ii) an area of 18.5 km^2 in the Campania region (Southern Italy, Fig. 3 and Fig. 4) in the municipality of Cervinara (Avellino province) 30 km far from the regional capital Napoli and the Vesuvio volcano. The two areas were chosen for their common high tendency to rainfall induced shallow landslides, and concurrently the very different main genesis of the soil (disaggregation of an alpine chain in one case, sedimentation of volcanic products in the other) and climate conditions to whom they are exposed, that have determined the settlement of a different vegetation cover.

2.2. Valle d'Aosta

The Valle d'Aosta region (3200 km^2) is part of the alpine chain, passing through the principal Europe-vergent Austroalpine-Penninic structural domain of the Western Alps. The region presents a complete section of the orogenic prism including (i) the Austroalpine domain; (ii) the ophiolitic Piedmont zone; and (iii) the Pennidic domain. These tectonic-metamorphic units composed of a complex pile of nappes, which present a post-collisional tectonic activity and a neotectonic dislocation system activation (Bistacchi et al. 2001). The geomorphology of the study area is characterised by steep slopes and valleys shaped by glaciers. The glacial modelling is shown in the U-shape of the Lys and Ayas valleys, and the erosive depositional forms found in the Ayas Valley. The three valleys' watercourses, the Lys Creek, the Evançon Creek, and the Dora Baltea River, contributed to the glacial deposits modelling with the formation of alluvial fans.

The region is very prone to landslides due to the two main triggering factors represented by the high steepness of slopes and abundant mean annual precipitation (800–900 mm/y during the decade 2000–2009): rockfalls, deep-seated gravitational slope deformations, rocks avalanches, debris avalanches, debris flows, and debris slides are the main mass movements to which the area is subjected (Catasto dei Dissesti Regionale – from Val d'Aosta Regional Authorities). A fraction of 18 % (probably underestimated) of the Valle d'Aosta territory is affected by landslides (Trigila, 2007) and except in rare cases, every year multiple meteorological events causing landslides throughout the territory happen. Among the many historical triggering events that have affected the region, we recall here some of them by way of example: between the 26 and the 28 of April 2009 highly intense rainfall and snowfall had fallen in the Alert zone B causing multiple landslides (9 landslides of different types in the Alert zone B were reported, 26 landslides in the Region) a maximum of rainfall of 268 mm in three days was recorded by a meteorological station; a rainfall event between the 3rd and the 5th of May 2010 interested all the Region Val d'Aosta triggering multiple mass movements (13) of different nature, in the Alert zone b a maximum cumulative value of 188 mm of rainfall during the event was recorded; a month later, between the 14th and the 16th of June 2010, the Alert zone b was interested by another intense rainfall event causing 3 debris-flows and a couple of rockfalls, during the event a rainfall intensity of 20 mm/h and a maximum cumulative rainfall of 189 mm were recorded.

The massifs dominating the Valle d'Aosta landscape act as morphological boundaries and deeply influence the local climatic conditions. The high peaks limit the access of air masses from the Mediterranean Sea or the Atlantic Ocean, causing a clear difference in the rain and snow precipitation regimes (Mercalli, 2016). Indeed, the climate is characterized by wide range of temperatures and rainfall/snowfall (average values of 1000–1100 mm/year) in mountainous and marginal sector, while, in correspondence of the principal valley bottom, the weather conditions are associable to a temperate climate with relatively lower rainfall (lower than 600 mm/year).

As typical in alpine valleys, the study area has a prevalence of highly vegetated areas, while human settlement distribution is located at the valley bottom. The land cover is prevalently represented by forest, natural grassland, and rocky outcrops with little or no vegetation. Most common forest categories are mixed-coniferous forests (30 % of the total forested area), larch forests, mixed broad-leaved forests, and broad-leaved mixed coniferous forests. The coniferous trees are the most common, representing>90 % of the Aosta Valley forests: larch (Larix decidua Mill.), Norway spruce (Picea abies (L.) Karst,), Scots pine (Pinus sylvestris L.), cembra pine (Pinus cembra L.) and silver fir (Abies alba Mill.) are the dominant species (Camerano et al., 2007).

2.3. Cervinara

Due to the proximity to Vesuvio volcano, most of the Cervinara area presents typical layered soils composed by a basal layer of weathered bedrock (carbonates) covered by air-fall volcanic (pyroclastic) soils (Cuomo and Foresta, 2015; Cascini et al., 2011).Aside from the geomorphological, geological, and climatic characteristics (as aforementioned), there are two further reasons behind the choice of this area for the study: i) the availability of an abundant *in-situ* and laboratory dataset useful to define simulations input data; ii) the occurrence of relatively recent and well documented rainfall-induced shallow landslides, being the latter an essential condition for the validation phases.

In the mid of December 1999, the area of Cervinara was hit by intense rainfall that triggered several shallow landslides then evolved into debris flows and debris avalanches in the night between the 15th and 16th, causing six victims beside to severe damages to buildings and facilities. The intense rainfall event started on the 14th of December 12 a.m. The rain-gauge of the area (the S. Martino Valle Caudina rain gauge) recorded a cumulated rainfall of 264 mm in 38 h (Fiorillo et al. 2001; Fiorillo and Wilson 2004). Cascini et al. 2005 reported that the return time of the cumulated rainfall from the 14th of December 6:00p.m. to the 15th of December 6:00p.m. was 10–20 years, passing rapidly to an event with a return time of up to 50–100 years in the consecutive hours. During the night between the 15th and the 16th, in the time of three hours, multiple debris floods and flows were triggered in the municipality of Cervinara.

As aforementioned, the study area is characterized by pyroclastic soils over carbonate bedrocks, and frequently it is affected by flow-type rainfall-induced shallow landslides (Cascini et al., 2008). The pyroclastic soils (generally up to 2–3 m thick) derived from the explosive eruptions of Vesuvio volcano that has spread pumices and ashes over a surrounding area of 3000 km^2 (Cuomo and Foresta, 2015). From the granulometric point of view, the soils are mostly sands/gravels (the pumice soils) and silty sands/sandy silts (the ashy soils) (Bilotta et al., 2005). A typical stratigraphy of the area is ashy silty sands over ashy sandy silts, with eventual thin discontinuous layers of sands/gravels (pumices) embedded between the two, and carbonate bedrock below (Damiano et al. 2012). It is common to find also only the ashy silty sands soil over the bedrock or directly outcropping bedrock (Cuomo and Foresta, 2015). Geomorphologically, the area is characterized by

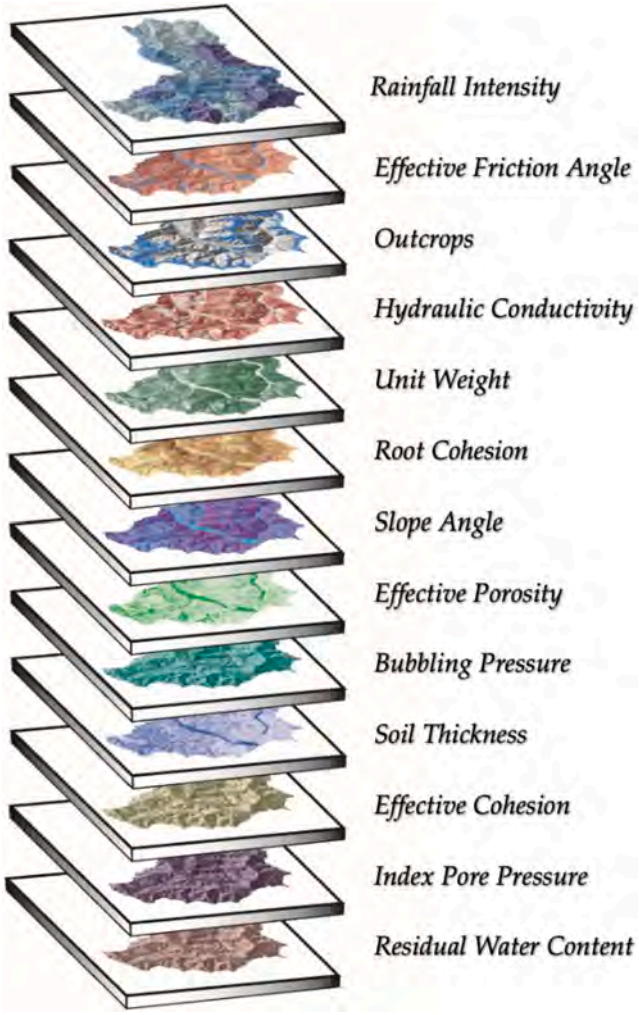

Fig. 5. HIRESSS input raster maps of Valle d'Aosta 'Alert zone b'.

bedrock concavities filled with pyroclastic materials reaching the maximum soil thickness in the central zone and planar hillslopes with an almost constant soil thickness (Cascini et al. 2008).

The vegetation of the Cervinara study area is dominated by beech woods and oak woods in the most elevated regions passing gradually to coppice and mixed woods of chestnut, yews, holm oaks, Italian alders, and Wych elm. In the areas close to the urban settlements are instead the small parcels of agricultural lands to dominate the landscape.

The weather condition to which the Cervinara territory is subjected are typical of the Temperate dry-warm summer climate: the main rainfall occurs in autumn and winter (maximum value 215 mm in December and 35 mm in July), the average monthly temperature reaches the highest values in July-August (24 °C) and the lowest in January-February (8 °C) (Fiorillo, 2011).

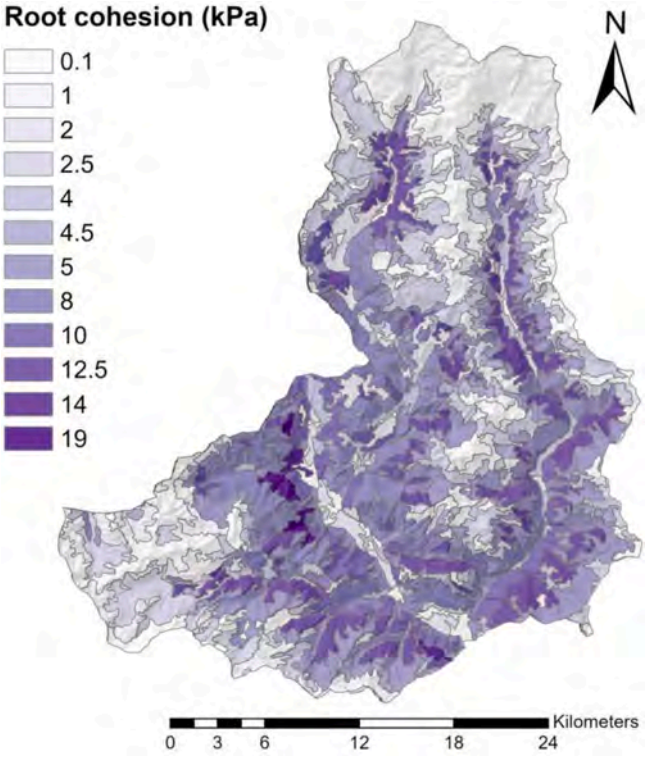

Fig. 6. Root cohesion values assumed for the Valle d'Aosta case study.

2.4. Data collection

HIRESSS considers static and dynamic parameters to perform the stability simulations. The static inputs are represented by geotechnical and morphological parameters of the areas, while the dynamic are represented by rainfall intensities. Spatial and temporal resolutions of input data and consequently the final outputs of simulation depend on the available information and the operator choices dictated by the requirements. HIRESSS loads the static and dynamic data as raster maps in which the parameters have been adequately spatialized (Fig. 5). All parameters considered are slope gradient, effective cohesion (c'), root cohesion (c_r), friction angle (φ'), dry unit weight (γ_d), soil thickness (dbt), hydraulic conductivity (k_s), initial soil saturation (S), pore size index (λ), bubbling pressure (h_b), effective porosity (n), residual water content (q_r), eventual outcrop rock mask and rainfall intensity.

Two field campaigns of soil sampling and superficial *in-situ* measurements had been conducted in August and September 2016, during which a total of 12 different sites had been investigated, to obtain necessary geotechnical data about the Valle d'Aosta case study (Fig. 2). Details about data collection from the *in-situ* surveys to the laboratory analyses and methods of data elaboration to product input maps had been depicted in Salvatici et al. (2018). Area of Cervinara case study had been widely investigated with *in-situ* tests including iron-rod drillings

Table 1
Valle d'Aosta case study: values of geotechnical parameters adopted for each lithological class in the slope stability simulations, where γ_d is the dry unit weight, n the effective porosity, c' the effective cohesion, φ' the friction angle, k_s the hydraulic conductivity, q_r the residual water content, λ the pore size index, h_b the bubbling pressure.

Lithological classes	*Soil Type*	*ϕ' (°)*	*c' (Pa)*	*γ_d (kN m^{-3})*	*n (%)*	*k_s (m s^{-1})*	*h_b (mH_2O)*	*q_r*	*λ*
Calcareous schist	Sand with gravelly silt	31	1000	16.5	39	1.1E-05	0.1466	0.041	0.322
Alluvial deposits	Sand with gravel and silt	26	1000	14.0	46	3.0E-06	0.1466	0.041	0.322
Glacial deposits	Sand with silty gravel	31	1000	15.3	41	2.7E-06	0.1466	0.041	0.322
Colluvial deposits	Sand with silty gravel	25	1000	13.7	47	2.5E-06	0.1466	0.041	0.322
Granites	Sandy gravel	30	1000	17.6	32	4.0E-06	0.1466	0.041	0.322
Mica schists	Sandy silty gravel	30	1000	17.7	32	6.0E-06	0.1466	0.041	0.322
Pietre Verdi	Gravel with silty sand	32	1000	16.3	37	4.6E-06	0.1466	0.041	0.322

Table 2
Geotechnical parameters input values for the Cervinara study area, where γ_d is the dry unit weight, n the effective porosity, c' the effective cohesion, φ' the friction angle, k_s the hydraulic conductivity, q_r the residual water content, λ the pore size index, h_b the bubbling pressure.

φ' (°)	c' (Pa)	γ_d (kN/m^3)	N (%)	k_s (m/s)	h_b (mH_2O)	q_r	λ
38	0	7.8	0.7	5.00E-06	0.8657	0.008	0.676

and penetrometer tests performed up to the bedrock contact beside to hand-excavated shafts to investigate 1 to 3 m below the ground surface (AdB-LGV (2013), further details of the field campaign are provided in Cuomo and Foresta (2015). For the geotechnical input data of the Cervinara case study (dry unit weight, effective porosity, effective cohesion, effective friction angle, saturated hydraulic conductivity, residual water content, pore size index, bubbling pressure) we referred to this work beside to Cuomo and Iervolino (2016). For the other input data, already available information was considered (DEM, soil thickness, rainfall intensity) or derived from exiting data through digital elaborations and analysis (slope angle, outcropping maps), except for the plant species distribution, for the determination of which, personally *in-situ* surveys had been integrated with Corinne Land Cover map 2012 information.

2.5. Static data

The geotechnical input data of the Valle d'Aosta case study originating from single points of sampling and measurements and literature data had been elaborated to obtain the necessary raster maps (Fig. 5) spatializing the information based on the lithology of the area (Salvatici et al., 2018). In Salvatici et al., 2018 data resulted from field campaign, laboratories analyses (accompanied with statistical information) and methods to spatialize the parameter have been presented and described. Values adopted for each lithology to perform the simulations are shown in Table 1.

Root cohesion variation map had been elaborated using for the plant species distribution the land use map Corine Land Cover 2012, 4th and 5th levels (ISPRA, 2018). Values adopted for the simulations are shown in Fig. 6.

In the Cervinara case study, existing slight differences in the fundamental geotechnical parameters from point to point within the 1–3 m of the soil, for the spatial distribution of the geotechnical parameters was chosen to consider a homogeneous layer covering all the area with the characteristics of an ashy silty sands layer (Damiano et al. 2012, Cuomo and Foresta, 2015). About the assumed soil thickness for this case study, the reported data by Cuomo and Iervolino (2016) regarding the pyroclastic deposits were considered. The slope angle was computed starting from a Digital Terrain Model (DTM) derived by LIDAR (Light Detection And Ranging) and provided by "Ministero dell'Ambiente e del Territorio". The DTM had a resolution of 1 m and was dated 2009. The outcrops map had been defined integrating aerial and satellite images of the interest period of rainfall event (google Earth images), soil thickness information (Cuomo and Iervolino, 2016) and the computed slope angles (the sectors with slope angle higher than 60° have been considered outcropping rocks).

Based on data reported by Billotta et. al, 2005, Cuomo and Foresta (2015), Cuomo and Iervolino (2016), and (Cuomo et al., 2021), for the homogeneous layer the following values of the geotechnical parameters were assumed: dry unit weight (γ_d) 7.8 kN/m^3, effective porosity (n) 0.7, effective cohesion (c') 0 kPa, effective friction angle (φ') 38°, saturated hydraulic conductivity (k_s) 5.00E-06 m/s, residual water content (q_r) 0.008, pore size index (λ) 0.676, bubbling pressure (h_b) 0.8657 mH_2O (Table 2).

The soil thickness data reported by Cuomo and Iervolino, 2016 for the pyroclastic deposit show values ranging mainly between 0 m and 5 m, in very few areas the soil is reported to reach 10 m of depth. The slope angle derived from the 1-meter resolution DTM shows values ranging from 0° to 83°. The total masked area representing outcropping rock sectors covers a surface of 1.5 km^2.

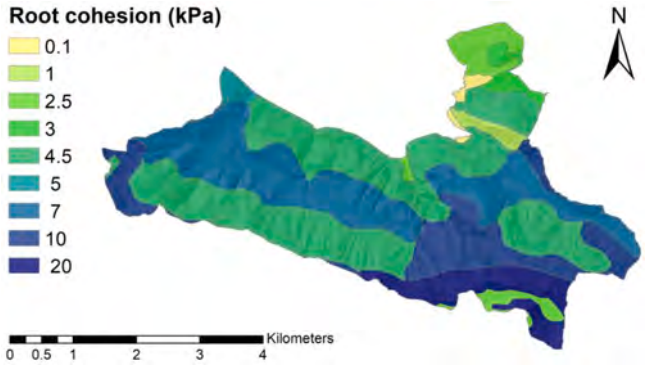

Fig. 7. Root cohesion values assumed for the Cervinara case study.

Table 3
The relative variations of each parameter considered in the Monte Carlo simulations.

Parameters	*Range of variation*
Cohesion	40 %
Friction angle	20 %
Slope	20 %
Dry soil unit weight	21 %
Hydraulic conductivity	60 %
Pore size index distribution	30 %
Bubbling pressure	20 %
Porosity	20 %
Residual water content	30 %
Root cohesion	50 %

The root cohesion values assumed for the area range from a minimum of 0.1 kPa at the north-eastern border in correspondence of suburban areas to a maximum of 20 kPa at the south-eastern border in correspondence of forests dominated by beeches (Fig. 7).

For both the case studies HIRESSS was set to consider the ranges of variation reported in Table 3 for the parameters, and a uniform statistical distribution for all during the Monte Carlo simulations. Variation range for each parameter were chosen based on previous studies (Rossi et al., 2013; (Segoni et al., 2012); Tofani et al., 2017). The uniform distribution was set in order to limit bias due to a non-comprehensively knowledge of the distribution for different reasons in the two case studies: a not elevated number of samples for each lithology in the Valle d'Aosta case study caused by a very wide surface of the area (Salvatici et al., 2018); values inferenced for a unique shallow soil layer based on different studies (Billotta et. al, 2005, Cuomo and Foresta (2015), Cuomo and Iervolino (2016), and (Cuomo et al., 2021)) as aforementioned in the Cervinara case study.

2.6. Dynamic data

The dynamic data are constituted by the rainfall intensities, which are read by the model to compute for every time step the soil saturation and consequently matrix suction and pressure head of every pixel. Initial soil saturation distribution could be provided to the model if available. Otherwise, it is possible inserting an initial soil saturation of zero for every pixel of the area, the model starts from zero and through the hydrological equations on which is based computes the soil saturation for every time step. It is worthwhile mention here that being a soil saturation of zero not realistic even for very permeable coarse soil, particularly in the climate conditions of the study areas, it is essential to have a sufficient backward extension of the rainfall data with respect to an

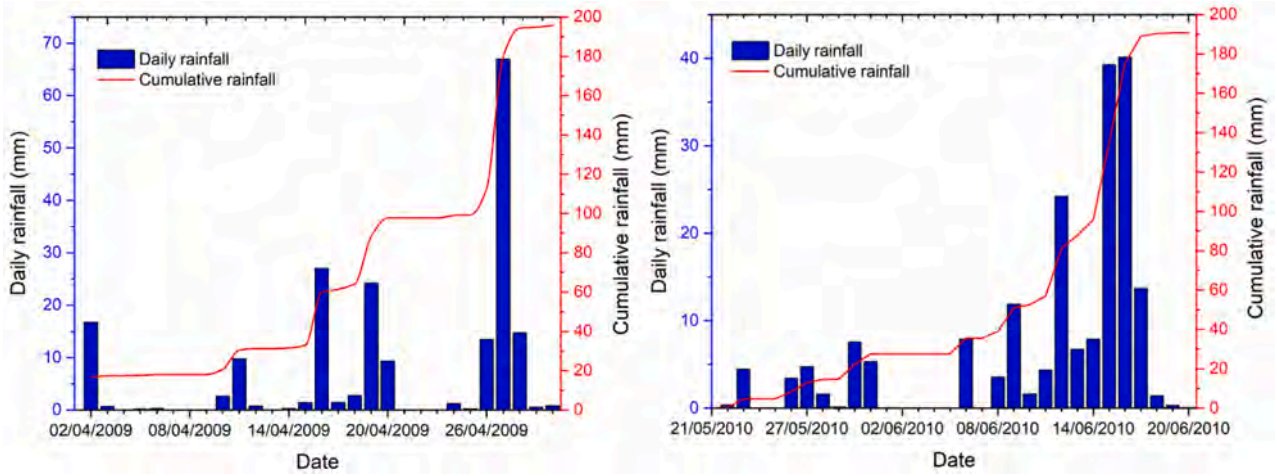

Fig. 8. Valle d'Aosta case study: intensity rainfall per day and cumulative rainfall for the event from the 2nd and the 30th of April 2009 (left) end the event from the 21st and the 20th of June 2010 (right). Daily and cumulative rainfall referring to the whole area had been calculated as mean values of the data registered by the 27 rain gauges.

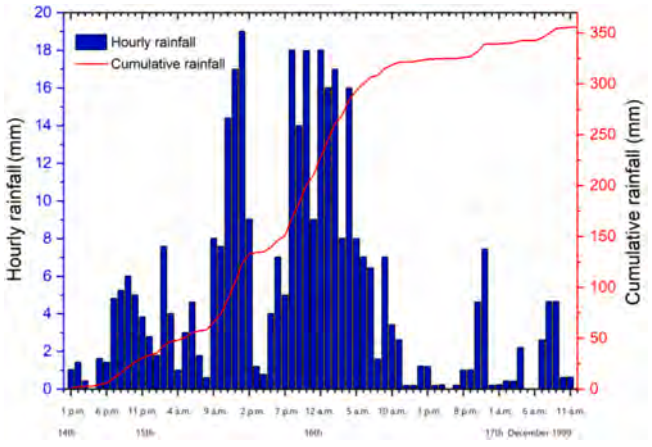

Fig. 9. Cervinara case study, hourly and cumulative rainfall of a three days event in December 1999.

eventual particular period of interest of the simulation, to be sure that the saturation conditions reconstructed by the hydrological model are very barely influenced by the fictious initial soil saturation.

In the study area of the Valle d'Aosta, the hourly rainfall data from 27 rain gauges were available. The rainfall data had been elaborated applying the Thiessen polygon methodology (Rhynsburger, 1973) modified to consider catchment basins to spatialize the data set and generate the raster maps (Salvatici et al., 2018). Two different periods of rainfall have been considered to perform the stability simulations (Fig. 8): i) 02/04/2009–30/04/2009; ii) 21/05/2010–20/06/2010.

In the Cervinara case study rainfall data of a unique rain gauge were available. The period of rainfall considered for the simulations is the time frame of three days at the turn of the night between the 15th of December and the 16th of December 1999, during which several landslides were triggered by intense rainfall. From the beginning of the considered period (14/12/1999, h 01.00 pm) to the end (17/12/1999, h 12.00) the rain gauge recorded a cumulative rainfall of 356 mm (Fig. 9). In the period two sharp rises in the rainfall intensity were recorded: from 9.00 15/12/1999 to 14.00 15/12/1999 in the area were fallen 75 mm of rainfall (on average 12.5 mm/h) with a peak of 19 mm from 13.00 to

Table 4
Simulations info: "Time step" represents the temporal resolution of the rainfall data; "Monte Carlo iterations" the number of iterations set for the simulation; "Root cohesion" indicates if the parameter was considered or not; "Processing time" is the time spent by Hiresss to complete the entire simulation; "FP maps 1 h, 24 h" hourly and daily number of output maps generated by HIRESSS (FP is Failure Probability).

Area	Period	Time step	Monte Carlo iterations	Root cohesion	Processing time	FP maps (1 h, 24 h)
Valle d'Aosta	02.04.2009-30.04.2009	1 h	100	No	423.381 min	725 (696, 29)
Valle d'Aosta	02.04.2009-30.04.2009	1 h	1000	No	2197.16 min	725 (696, 29)
Valle d'Aosta	02.04.2009-30.04.2009	1 h	10,000	No	18988.4 min	725 (696, 29)
Valle d'Aosta	02.04.2009-30.04.2009	1 h	10	Yes	322.516 min	725 (696, 29)
Valle d'Aosta	02.04.2009-30.04.2009	1 h	100	Yes	461.173 min	725 (696, 29)
Valle d'Aosta	02.04.2009-30.04.2009	1 h	1000	Yes	2345.83 min	725 (696, 29)
Valle d'Aosta	02.04.2009-30.04.2009	1 h	10,000	Yes	21039.5 min	725 (696, 29)
Valle d'Aosta	20.05.2010-20.06.2009	1 h	1000	No	2471.41 min	802 (770, 32)
Valle d'Aosta	20.05.2010-20.06.2009	1 h	1000	Yes	2627.56 min	802 (770, 32)
Cervinara	14.12.1999-17.12.1999	1 h	1000	No	22.73 min	76 (72, 4)
Cervinara	14.12.1999-17.12.1999	1 h	1000	Yes	25.05 min	76 (72, 4)

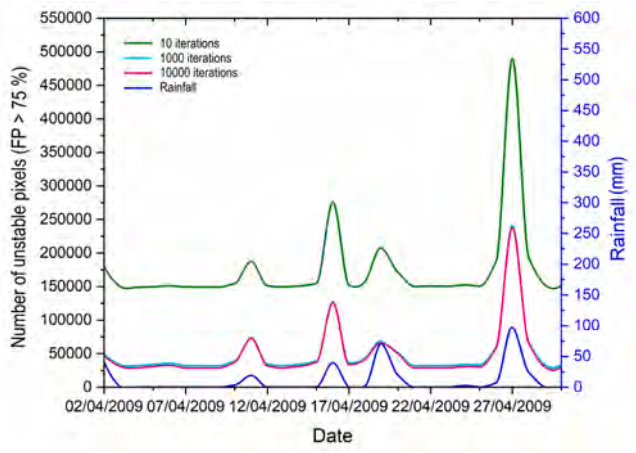

Fig. 10. 2009 Valle d'Aosta event, results of simulations with a different number of Monte Carlo iterations. Colored curves represent trend of unstable pixels (resulting having a daily max failure probability higher than 75%).

14.00; from 18.00 15/12/1999 to 5.00 16/12/1999 a cumulative rainfall of 154 mm was recorded (on average 12.8 mm/h) with three peaks around to 18 mm/h.

2.7. Results

Multiple simulations had been conducted for both the study areas integrating or not the contribution of the root cohesion to compare the results and analyze the effect of the latter on the failure probabilities computed by the model. During the research process, 11 simulations had been completed, of which 9 relating to the Valle D'Aosta area and two to Cervinara area (Table 4).

About the Valle d'Aosta case study, two different periods of rainfall had been simulated multiple times, setting the model for different numbers of iterations, and inserting or not the root cohesion. Event from the 2nd of April 2009 to the 30th of April 1999 was simulated 7 times, three times not including the root cohesion and setting the number of iterations to 100, 1000, 10000, and 4 times including the root cohesion and setting the number of iterations to 10, 100, 1000, 10000. The event from the 20th of May 2010 to the 20th of June 2010 had been simulated two times, setting both the times the number of iterations to 1000, with the difference of inserting or not the root cohesion. About the Cervinara case study, one rainfall event was simulated (14.12.1999 – 17.12.1999) two times, with 1000 Monte Carlo iterations in both cases, and inserting or not the root cohesion.

Before proceeding with all the other planned simulations, a study on the preferable number of Monte Carlo iterations had been performed. The Monte Carlo iterations performed by HIRESSS to manage the spatial uncertainty of the input parameters is a fundamental aspect of the forecasting procedure, the setting of which strongly affects the resulting failures probabilities. The higher the number of iterations, the higher the reliability of the forecasts. On the other hand, a higher number of iterations considerably slows down the processing calculations, so that the question here is finding the best compromise between processing time and reliability of the results.

To identify appropriate number of iterations in the context of the present research, four simulations of the Valle d'Aosta 2009 event were performed with the same input values of the parameters but varying the number of iterations (10, 100, 1000, 10,000 shoots). The simulation results had been then compared, considering the number of unstable pixels computed in the three cases for the same days of the event and the processing times (Fig. 10). Hereinafter, please note that the precautionary value of 1.2 for the factor of safety and the 80 % for the failure probability (FP) were chosen as thresholds to consider unstable a pixel: during the iterative process, for each pixel and time step, the model computes the factor of safety for a certain number of times (configurable). The model was set to consider unstable a pixel when the calculated factor of safety results lower than the value of 1.2: if a pixel shows a FP higher than the 80 % in a certain time step means that the model found>80 times out of 100 a factor of safety lower than 1.2 for that pixel in that time step. FP threshold to consider unstable a pixel should be set case to case depending on the purposes of the slope stability analysis. The threshold of 80 % was chosen based on previous HIRESSS applications ((Rossi et al., 2013); Salvatici et al., 2018) and considering aims of the research; in the present study, it has been used to plot and describe trends of the simulations and in some comparative analyses described further in the text. It is worthwhile mentioning here that some comparative analyses have also been carried out considering the entire specter of the failure probabilities, to better explore the behavior of the simulations with and without the root cohesion.

The difference between the 10-simulation and the 100-simulation resulted about 100,000 fewer unstable pixels for the latter, while between the 100-simulation and the 1000-simulations there were 25,000 pixels of difference on average (also in this case the simulation obtained through a higher number of iterations showed less unstable pixels) (Fig. 10). Differently, the differences between the 1000-simulation and the 10000-simulation were so little to be considered negligible, against a considerable difference in terms of processing time. Indeed, the 1000-simulation needed 2346 min (39 h) to be completed, while the 10000-simulation took 21,039 min (350 h). The convergence of the results and the quite different processing times lead to the choice of 1000 iterations for the successive simulations.

Simulation results are shown in Table 5 in the form of summary statistics about count of unstable pixels, i.e., number of pixels computed by HIRESSS as having a daily max FP higher than 80 %. In table have been reported for each simulation total count of unstable pixels over the period (Sum), average unstable pixels per day (Mean), count of unstable pixels of the most stable day during the period (Minimum), count of unstable pixels of the most unstable day during the period (Maximum).

Table 5
Count of unstable pixels (pixels with a daily max failure probability higher than 80%) of each simulation. The "Sum" is the total count over the period, "Mean" the average unstable pixels per day, "Minimum" represents the count of unstable pixels of the most stable day during the period, "Maximum" is the count of unstable pixels of the most unstable day during the period.

Area	Event	Simulation (root cohesion, iterations)	Sum	Mean	Minimum	Maximum
Valle d'Aosta	2009	No, 100	2,082,630	71,815	52,229	299,607
		No, 1000	1,452,730	50,094	31,857	240,611
		No, 10,000	1,381,390	47,634	28,614	237,416
		Yes, 10	5,067,920	174,756	148,883	489,794
		Yes, 100	2,082,760	71,819	52,114	299,641
		Yes, 1000	1,452,540	50,088	31,864	240,775
		Yes, 10,000	1,381,410	47,635	28,611	237,404
Valle d'Aosta	2010	No, 1000	1,650,370	51,574	31,359	146,212
		Yes, 1000	1,649,960	51,561	31,389	146,012
Cervinara		No, 1000	809	202	0	463
		Yes, 1000	808	202	0	462

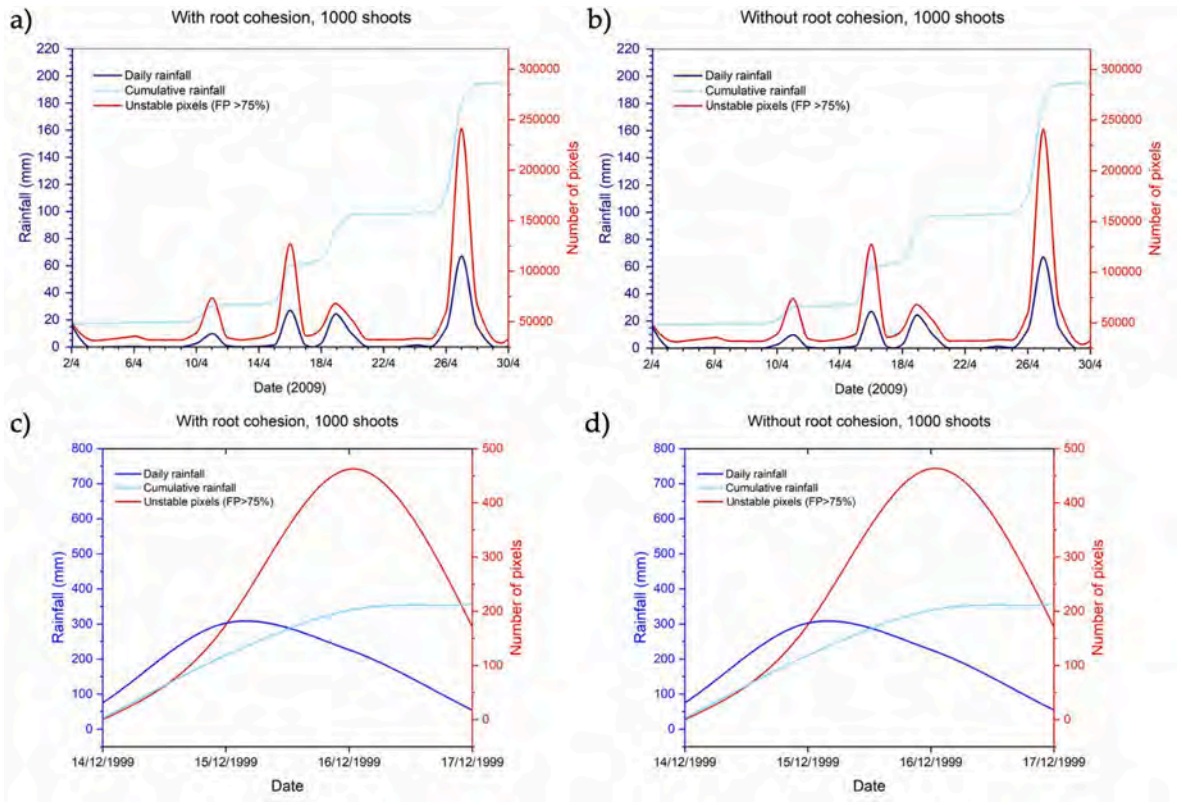

Fig. 11. Unstable pixels (pixels with a daily max failure probability higher than 80 %): a) and b) simulations of 2009 Val d'Aosta event with root cohesion integrated or not respectively, 1000 Monte Carlo iterations both; c) and B) simulations of 1999 Cervinara event with root cohesion integrated or not respectively, 1000 Monte Carlo iterations both.

In Fig. 11 trend of unstable pixels during the period of simulation is shown for 2009 Val d'Aosta event (1000 iterations) and 1999 Cervinara event with integration or not of the root cohesion into the model, in the plots the daily and cumulative rainfall are also reported. Rainfall data plotted for Valle D'Aosta represent the average rainfall per polygon recorded by the rain gauges of the study area during the period of the simulation. For Cervinara, the reported rainfall refers to data recorded by the only rain gauge present in the area. Same plot had been generated for each simulation performed.

In Fig. 11 the daily differences of unstable pixels between a) and b), and between c) and d) are little so that the graphs seem apparently identical. To appreciate the differences between the simulations considering or not the root reinforcement effect, results had to be profoundly analyzed and consequently plotted as presented in the following discussion section.

3. Discussions

The main scope of the present study was to analyze the effect of the root cohesion on the simulation results, by means of comparative analyses and validation of the results. First step of the comparative analyses consisted in the examination of the results of the simulations considering the unstable pixels trend during the rainfall periods simulated. As aforementioned, 1.2 for the factor of safety and 80 % for FP were used as thresholds to consider unstable a pixel during the present study. Further in the text comparative analyses considering also the entire specter of the failure probabilities are presented.

Trends of unstable pixels (pixels with a daily max FP higher than 80 %) together with daily and cumulative rainfall (Fig. 11) allowed to have a preliminary and overall view of the behavior of the model during the different simulations. Beside the expectable peaks of unstable pixels in correspondence of rainfall peaks, in Fig. 11 it is possible to observe in the Valle d'Aosta case study the behavior of the model in case of two close-up rainfall peaks: when two close-up rainfall peaks of comparable size occurred, in correspondence of the second rainfall peak there was a less intense increase in the number of unstable pixels compared to the answer of the model for the first one (Valle d'Aosta 2009-event, rainfall peaks of the 16th April and the 19th April). Differently, when the second peak is considerably higher than the first, the trend of unstable pixels returned to reflect the rainfall path closely. This behavior reflects the physical models (geotechnical and hydrological) of HIRESSS, shaped on the dynamics of the rainfall triggered shallow landslides, for which abrupt rainfall after days of drought have a higher impact compared to the same number of precipitations following days of rainfall. However, when the rainfall is abundant, even if it follows other days of precipitations, the impact returns to be high for the trigger of shallow landslides.

Regarding the aspects more closely concerning the present study, the comparison of count (Table 5) and trend of unstable pixels (Fig. 11) of the simulations with and without the root cohesion represented the first step to analyze the effect of the integration on the failure probabilities computed by the model. Since only the comparisons between simulations with an equivalent number of iterations and referring to the same area and rainfall period are meaningful in the context of this analysis, the comparisons could concern the three pairs of the Valle d'Aosta 2009-event (100, 1000, 10,000 iterations), the pair of the Valle d'Aosta 2010-event (1000 iterations) and the pair of the Cervinara event (1000 iterations).

Since the effect of the root reinforcement was introduced into the model in the form of an additional cohesion, comparing simulations with or without the root cohesion, we expected to find a higher number of unstable pixels in the simulations in which the contribution of the root cohesion was not considered. Considering the total unstable pixels counted by the model during the simulations, there were more unstable

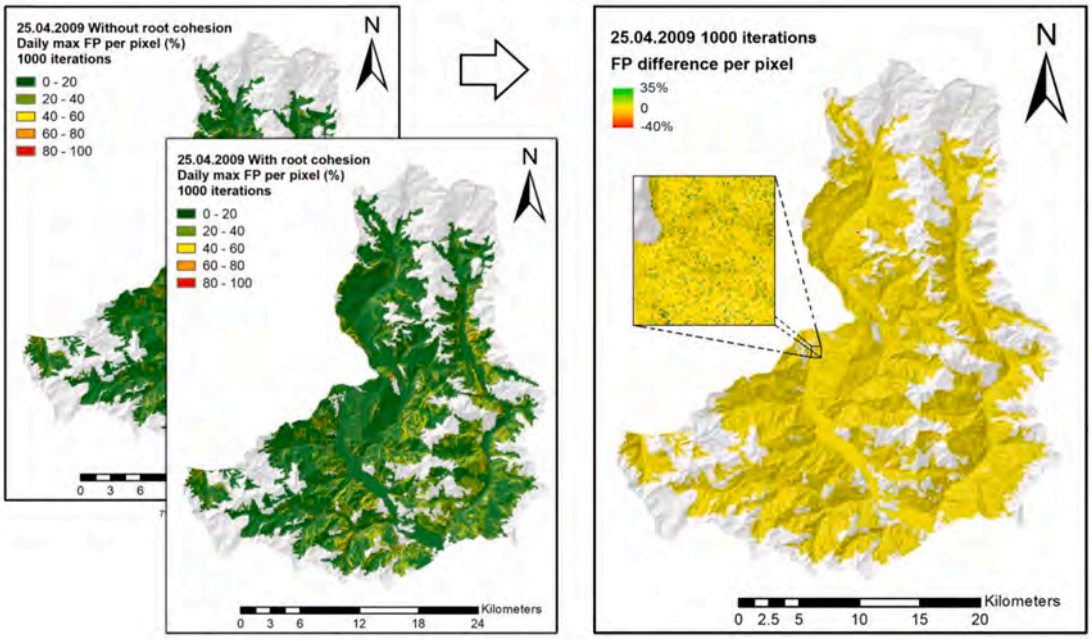

Fig. 12. FP maps of Valle d'Aosta case study for the 25th of April 2009. Left: daily max FP per pixel of the simulation without the root cohesion and daily max FP per pixel of the simulation with the root cohesion. Right: FP difference per pixel (for each pixel, daily max FP of the simulation without the root cohesion minus daily max FP with the root cohesion).

pixels in the simulation without the root cohesion in three comparisons out of five (Valle d'Aosta 2009-event 1000 iterations, Valle d'Aosta 2010-event and Cervinara event). In the other two cases (Valle d'Aosta 2009-event 100 and 10,000 iterations) the model found a higher overall number of unstable pixels in the simulation in which the contribution of the root cohesion was considered. Even considering the mean, maximum and minimum values of unstable pixels per day (Table 5), a higher tendency to the instability of the simulations without the root cohesion did not emerge. Examining the results through this approach and considering 80 % as threshold probability for failure, expectations were only partially respected.

Simulations results had been then compared i) from the point of view of the difference in the failure probabilities pixel by pixel between the simulations with and without the root cohesion during rainy and not rainy days; ii) analyzing the trend of the unstable pixels difference (count of unstable pixels of the without root cohesion-simulation minus the count of the with root cohesion-simulation) during the whole period of the simulations in different subareas of the case studies; iii) examining the trend of the failure probabilities (comparison of the number of unstable pixels for each FP of the simulations with and without the root cohesion) in rainy and not rainy days in different subareas of the case studies.

3.1. *Differences in the failure probabilities pixel by pixel*

For both the case studies, one not rainy day and one rainy were selected to analyze the difference between the simulations with or without the root cohesion in terms of FP at the level of each pixel. For each selected day, a raster difference was performed, subtracting the FP of each pixel of the map with the root cohesion to the FP of the correspondent pixel of the map without the root cohesion, so that obtaining the difference in the max FP computed by the model. Finally, the mean difference at the basin level was calculated.

For the Valle d'Aosta case study-two days of the 2009-event were selected, the 25th of April as the not rainy day and the 27th of April as the rainy day. The raster difference of the daily max FP was performed twice for this case study, considering the 1000 iterations-simulation and the 10,000 iterations-simulation.

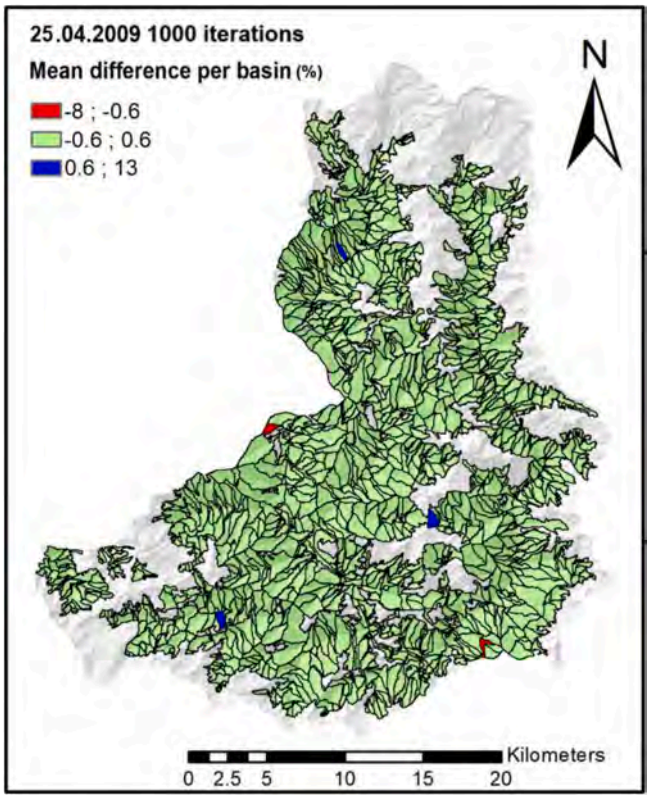

Fig. 13. Mean Failure Probability (FP) difference between the two simulations (mean of the difference: max FP of the simulation without the root cohesion minus max FP of the simulation with the root cohesion) at the basin level in the not rainy day (25.04.2009), Valle d'Aosta case study, 1000 Monte Carlo iterations.

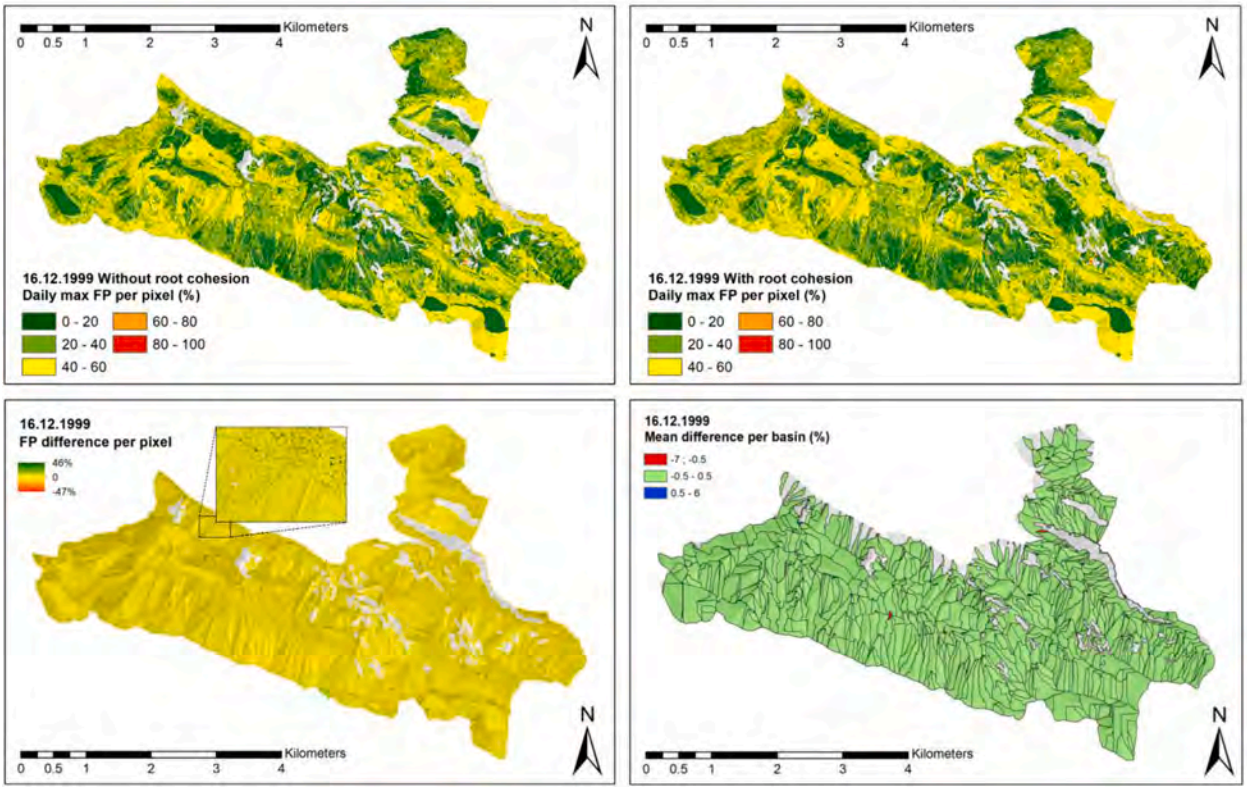

Fig. 14. FP maps of Cervinara case study for the 16th of December 1999: a) daily max FP per pixel of the simulation without the root cohesion; b) daily max FP per pixel of the simulation with the root cohesion; c) FP difference per pixel (for each pixel, daily max FP of the simulation without the root cohesion minus daily max FP with the root cohesion); d) FP mean difference per basin.

Raster difference maps of the rainy day and the not rainy day of the 2009 Val d'Aosta event resulted dominated by difference values close to zero in both cases of 1000 and 10,000 iterations. As example, in Fig. 12 is shown the 1000 iterations-simulation raster difference map of the 25th of April: predominance of the pixels in the spectrum of the yellow is clear, indicating globally a prevalence of low differences in the percentage of the FP of the pixels belonging to the simulations with or without the root cohesion. Furthermore, regarding the pixels deviating from the yellow, there is no marked trend towards red (which indicates a greater probability of failure in the simulation with root cohesion) nor towards green (which indicates a greater probability of failure in the simulation without root cohesion).

The four raster difference maps (relate to 25th April and 27th April of the 1000 and 10,000 iterations simulations) had been analyzed obtaining the mean difference per territorial unit -sub-basin- (i.e., it had been calculated within the borders of each sub-basin the mean difference of the FP of the pixels between simulation without the root cohesion and simulation with the root cohesion) (Fig. 13). Mean FP difference per sub-basin of the 1000 iterations-simulation varied between −8 % and 13 %, but only in sporadic cases the sub-basins reached these values, almost the totality of the basins showed a value close to zero (falling into the range −0.6 %, 0.6 %) in both days. Mean FP difference per sub-basin of the 10,000 iterations-simulation showed a smaller range of variation (-1 %, 1 %), and almost the totality of the sub-basins had a mean value around zero (falling into the range −0.5 %, −0.5 %) also in these cases.

In the Cervinara case study, the 14th of December 1999 was individuated as not rainy day and the 16th of December as rainy day (only 1000 iterations-simulation here). Apart from the predictable massive variation in the maximum probability of failure of the area from 14th to 16th (Fig. 14), also in this case, the differences between the probability of pixel failure of the simulations with or without root cohesion resulted negligible. Almost the totality of the sub-basins showed a mean value of the differences between −0.5 % and 0.5 %, in sporadic cases reached values falling in the ranges of −4 %, −0.5 % and 0.5 %, 4 % in the not rainy day and values falling in the ranges of −7 %, −0.5 % and 0.5 %, 6 % in the rainy day (Fig. 14).

Table 6
Case studies of the unstable pixels difference analysis.

Event	Number of iterations	Area
Valle d'Aosta 2009	1000	Whole area
Valle d'Aosta 2009	10,000	Whole area
Valle d'Aosta 2010	1000	Whole area
Valle d'Aosta 2010	1000	Subarea of uniform lithology (uniform geotechnical parameters values)
Valle d'Aosta 2010	1000	Subarea with uniform root cohesion value (19 kPa)
Valle d'Aosta 2010	1000	Subarea of uniform lithology and root cohesion value (12.5 kPa)
Valle d'Aosta 2010	1000	Subarea with root cohesion values higher than a threshold (10 kPa)
Cervinara	1000	Whole area

Adopting this approach of analysis of the results and dealing with failure probabilities (not with factors of safety), we could not detect significant differences at the sub-basin level between the results of the simulations with or without the root cohesion in both the case studies.

3.2. *Unstable pixels trend (whole period)*

The second approach of analysis consisted in the examination of the trend of the unstable pixels difference (for each day of the event, count

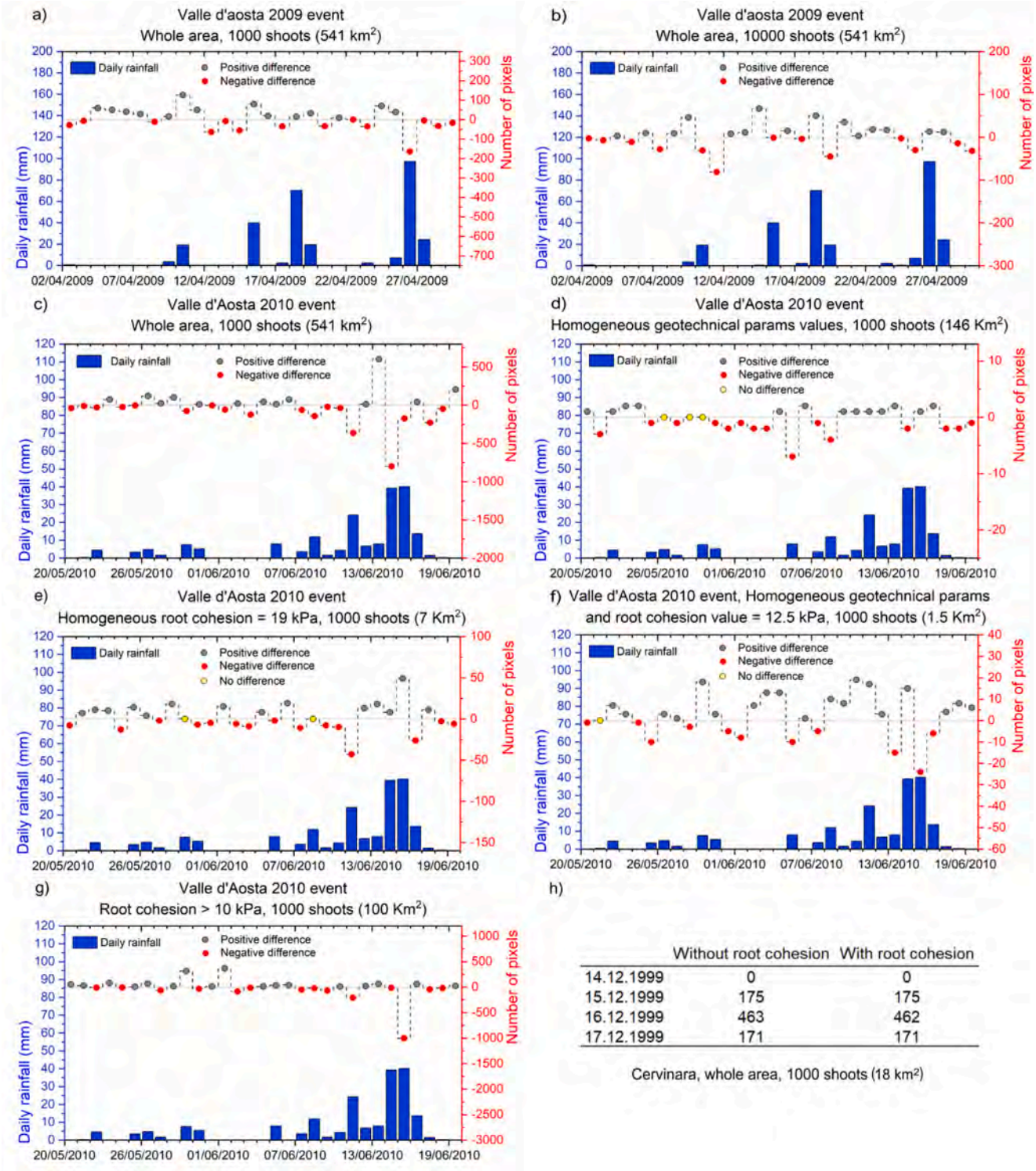

	Without root cohesion	With root cohesion
14.12.1999	0	0
15.12.1999	175	175
16.12.1999	463	462
17.12.1999	171	171

Cervinara, whole area, 1000 shoots (18 km²)

Fig. 15. Unstable pixels difference - for each day of the event, count of unstable pixels of the simulation without root cohesion minus the count of unstable pixels of the simulation with root cohesion (unstable pixels are the ones resulted having a daily max failure probability higher than 80 %) – of 8 different cases.

of unstable pixels of the simulation without root cohesion minus the count of unstable pixels of the simulation with root cohesion, unstable pixels are the ones resulted having a daily max FP higher than 80 %) during the whole period of the rainfall event simulated, to compare day by day the two simulations (without the root cohesion/with the root cohesion).

Present approach of analysis considered the Valle d'Aosta 2009 event-1000 iterations; the Valle d'Aosta 2009 event-10000 iterations; the Valle d'Aosta 2010 event (1000 iterations); the Cervinara event (100 iterations). In addition, to explore better the root cohesion impact, the results of the Valle d'Aosta 2010 event had been elaborated to analyse the difference trend in subareas with selected characteristics. Unstable pixels difference trend analysis had been carried out dealing with the 8 cases summarized in Table 6. Resulting trends are presented in Fig. 15.

Unstable pixels trend difference relating to the whole area in three different simulations (Fig. 15 a, b, c) resulted not positioning clearly

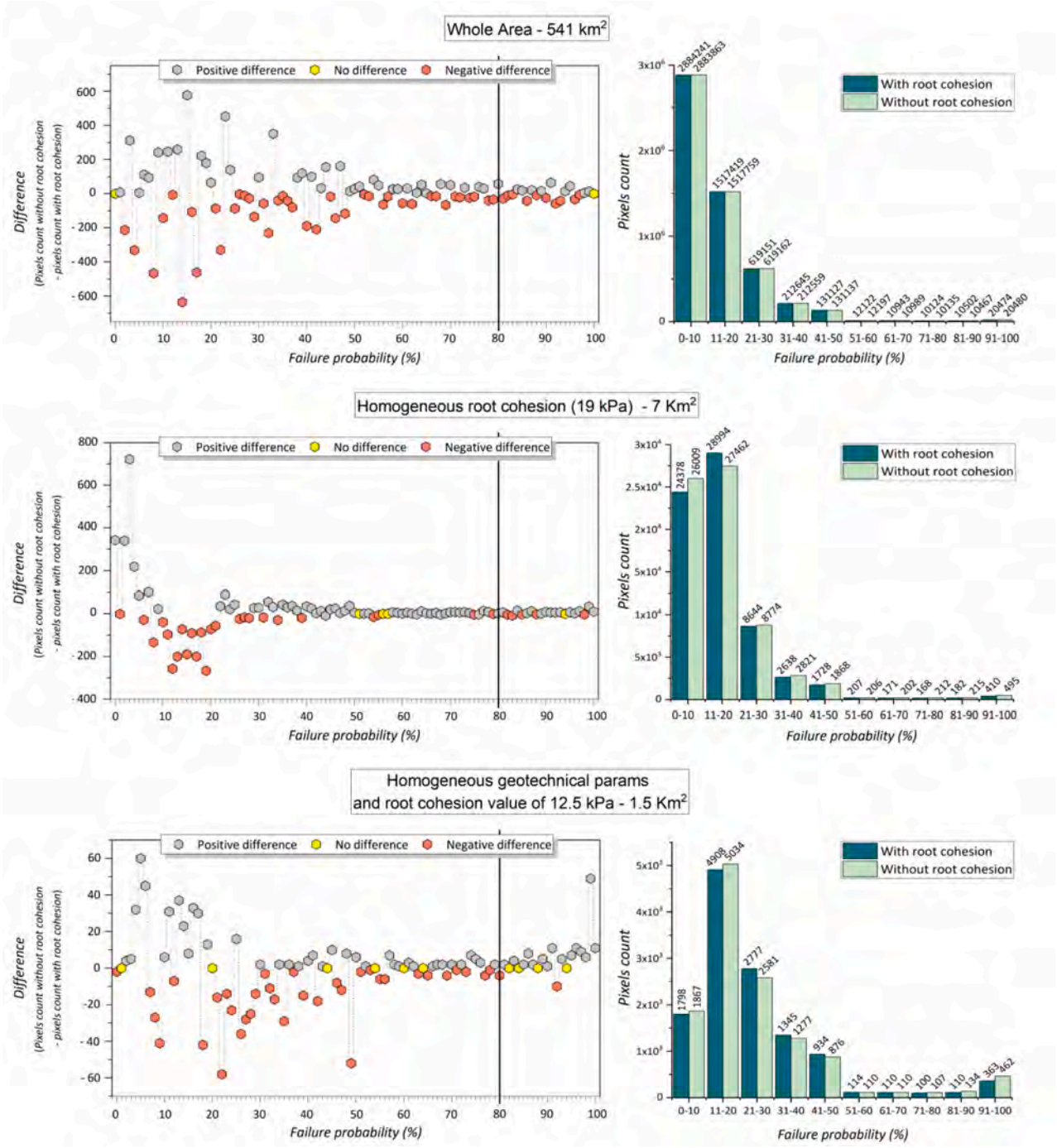

Fig. 16. Failure probability (FP) trend for the "not rainy day" (08.04.2009) of the simulations with and without the root cohesion in three different areas: a) the whole area; b) a subarea characterized by a root cohesion mean value of 19 kPa; c) a subarea with same values of geotechnical parameters and root cohesion of 12.5 kPa. On the left: colored hexagons represent the difference between the simulations: for each FP, pixels count found by HIRESSS having that FP in the simulation without the root cohesion minus pixels count with same FP found in the simulation with the root cohesion. On the right: bars with labels for intervals of FP from 0 % to 100 % (ten intervals 10 % wide) describing count of pixels found by the model having FP falling in each interval in the two different simulations.

above or below the non-difference line (every day in which a point representing the difference is placed below the zero line -in grey color- HIRESSS found more unstable pixels in the simulation with the root cohesion) but in the majority of the days the difference resulted negative. In these cases, the 54 %, 61 % and 60 % of the days (respectively in the simulations of Valle d'Aosta case study 2009–1000 iterations, 2009–10000 iterations and 2010–1000 iterations) the difference resulted negative.

In the three cases in which some areas have been selected considering the root cohesion values - subarea with uniform root cohesion value of 19 kPa, subarea of uniform lithology and root cohesion value of 12.5 kPa, subarea with root cohesion values higher than threshold of 10 kPa - the percentages of days about which the difference resulted negative dropped to 50 %, 37 %, 47 % respectively. The case in which the root cohesion effect emerged more distinctly, i.e., in which the difference resulted positive in the 63 % of the days (Fig. 15 –e) was the one in which an area with homogeneous root cohesion values of 12,5 kPa and homogenous geotechnical parameters values have been

Table 7
Valle d'Aosta case study, 2009 event. Comparisons of the unstable pixels of the simulation without and with the root cohesion: a) count of the pixels with FP > 80 % in the area; b) percentage of the pixels with a FP > 80 % normalized to the area.

Area	With root cohesion		Without root cohesion	
	Not rainy day			
	a	b	a	b
Whole area	31,901	0.5876 %	31,930	0.5882 %
Root cohesion = 19 KPa	607	0.90 %	727	1.06 %
Same geotechnical params and root cohesion = 12.5 kPa	485	3.87 %	604	4.82 %
	First rainy day			
	a	b	a	b
Whole area	234,103	4.312 %	233,959	4.310 %
Root cohesion = 19 KPa	4245	6.21 %	4276	6.26 %
Same geotechnical params and root cohesion = 12.5 kPa	2012	16.02 %	2008	15.99 %
	Second rainy day			
	a	b	a	b
Whole area	64,851	1.195 %	64,737	1.192 %
Root cohesion = 19 KPa	1195	1.75 %	1190	1.74 %
Same geotechnical params and root cohesion = 12.5 kPa	839	6.68 %	841	6.70 %

considered.

In the Cervinara case study, the count of unstable pixels (max FP > 80 %) per day of the simulations with or without the root cohesion resulted having an equivalent trend in the two cases. We preferred to present the results in the form of a table instead of the plots presented for the Valle d'Aosta case study. As shown in Fig. 15h, in terms of count of unstable pixels there is no difference except for one day out of three (16.12.1999) consisting of only one pixel: 463 unstable pixels in the simulation without the root cohesion, 462 in the simulation with the root cohesion.

These findings suggest that the root cohesion moved the results of the simulations towards higher stability, but its effect is not clearly detectable when we considered the whole area. Up to this point of the work, we have discussed the results only referring to failure probabilities higher than the 80 %, the examination of the difference trend considering the whole spectrum of failure probabilities could give more comprehensive indications, this is the rationale of the successive analysis approach.

3.3. Failure probability trend (rainy and not rainy days)

The third approach to analyze the effect of the root cohesion consisted in comparing the number of unstable pixels found by the model for each FP value (from 0 to 100 %) in the simulations with and without the root cohesion, during rainy and not rainy days and in different subareas with specific features. For the Valle d'Aosta case study, the analysis was performed on the results of 2009 event – 1000 iterations of three different areas: a) the whole area; b) a subarea of homogeneous root cohesion of 19 kPa; c) a subarea of homogenous lithology (i.e., homogenous values of the geotechnical parameters) and root cohesion value 12.5 kPa. The selected days are the 08.04.2009 as the "not rainy day" (a day without precipitations following days without precipitations), the 27.04.2009 as "first rainy day" (a day with rainfall following days of no rainfall), the 28.04.2009 as "second rainy day" (a day with rainfall following a rainy day).

Simulations results had been processed to obtain the difference trend between the simulations in terms of number of pixels in the entire range of failures probabilities, i.e., for each FP was calculated the following difference: pixels count found by HIRESSS having that FP in the simulation without the root cohesion minus pixels count with same FP found in the simulation with the root cohesion. The difference was calculated for 9 different cases (three areas, three different days). In Fig. 16 are shown results of the analysis about the "not rainy day". Furthermore, total number of pixels with FP higher than 80 % was detected for each day, simulation and area. The unstable pixels (with FP higher than 80 %) found by HIRESSS in the 9 cases are shown in Table 7 - columns a) - while in columns b) are reported the percentages of the unstable pixels normalized to the respective area.

In the "not rainy day" (08.04.2009), the model found more unstable pixels in all the three areas in the simulation without the root cohesion, and the difference (between the count of unstable pixels of the two simulations) is higher in the two subareas with the same medium–high root cohesion (Table 7). About the entire range of failure probabilities, in the case of the whole area it was not possible to detect particular discrepancies between the two simulations. Differently in the subareas, we could observe an increasingly occurrence of positive differences with increasing of the failure probabilities, and higher number of pixels in the intervals of higher FP in the simulation without the root cohesion (Fig. 16). In the two rainy days the number of unstable pixels (FP higher than 80 %) for the two simulations resulted essentially the same in each case. Also considering the full range of FP, it was not possible to detect particular discrepancies in the behavior of the two simulations.

For the Cervinara case study, the analyses had been performed on the results regarding the whole area and the selected days were the 14th of December as a day with little rainfall and the 16th of December as day with abundant rainfall. In this case, we could not detect particular discrepancies between the simulations with or without the root cohesion nor in the number of unstable pixels (FP > 80 %) nor considering the difference for each FP, and this for both the days.

Basing on what have emerged, the effect of the root cohesion had a not negligible effect in the unsaturated conditions of the soil (not rainy day), while in saturated conditions the impact on the results in terms of failure probabilities was practically null. Considering the additional cohesion effect in HIRESSS undoubtedly produced higher values of factor of safety but considering the failure probabilities obtained through the Monte Carlo iterations it had a minimal impact, and this behavior was particularly clear when the saturated conditions were reached in the simulations. The root cohesion has been modelled as a component of the "standard" cohesion, consequently it was subjected to the same decrease of the latter in saturated conditions due to the increase of the denominator of the second term in the right member of equation (4). This is a reasonable approach supported by the literature that reported decreases in the root cohesion as the soil moisture increases (Lian et al. 2019; Hales and Miniat, 2017; Pollen, 2007) and adopted by several authors (e.g., (Chok et al., 2015) ; Preti and Giadrossich, 2009; Hales and Miniat, 2017). But, considering that the stabilizing action of vegetation in the saturated condition is indisputable when dealing with shallow mass movements, the model of the root cohesion assumed to consider the parameter in HIRESSS might not be the most suitable for the shallow landslides, in the context (vegetation, weather conditions, soil types) of the study areas of this research.

3.4. Validation

As conclusive phase of the evaluation of the root cohesion effect, the eventual improvements obtained in the forecasting capabilities of HIRESSS were assessed validating the results considering the landslides occurred in the simulated periods.

One of the most useful applications for which a distributed model capable of quick processing can be used is the landslides forecasting at a regional scale, to support territory authorities and civil protection agencies in making decisions aimed to protect people and infrastructures from the hydrogeomorphic events. In this perspective, the FP of each pixel is a redundant information not practical to use. Rather, the results should be synthesized through a chosen criterium and expressed in the form of failure probabilities of more extended areas like the basins of a

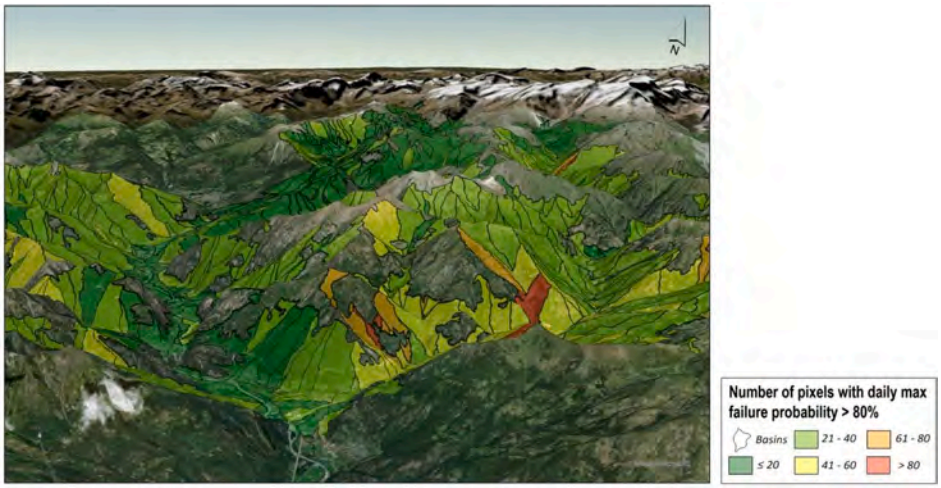

Fig. 17. Pixels FP synthesized into number of unstable pixels per basin. Valle d'Aosta study area, 27.04.2009.

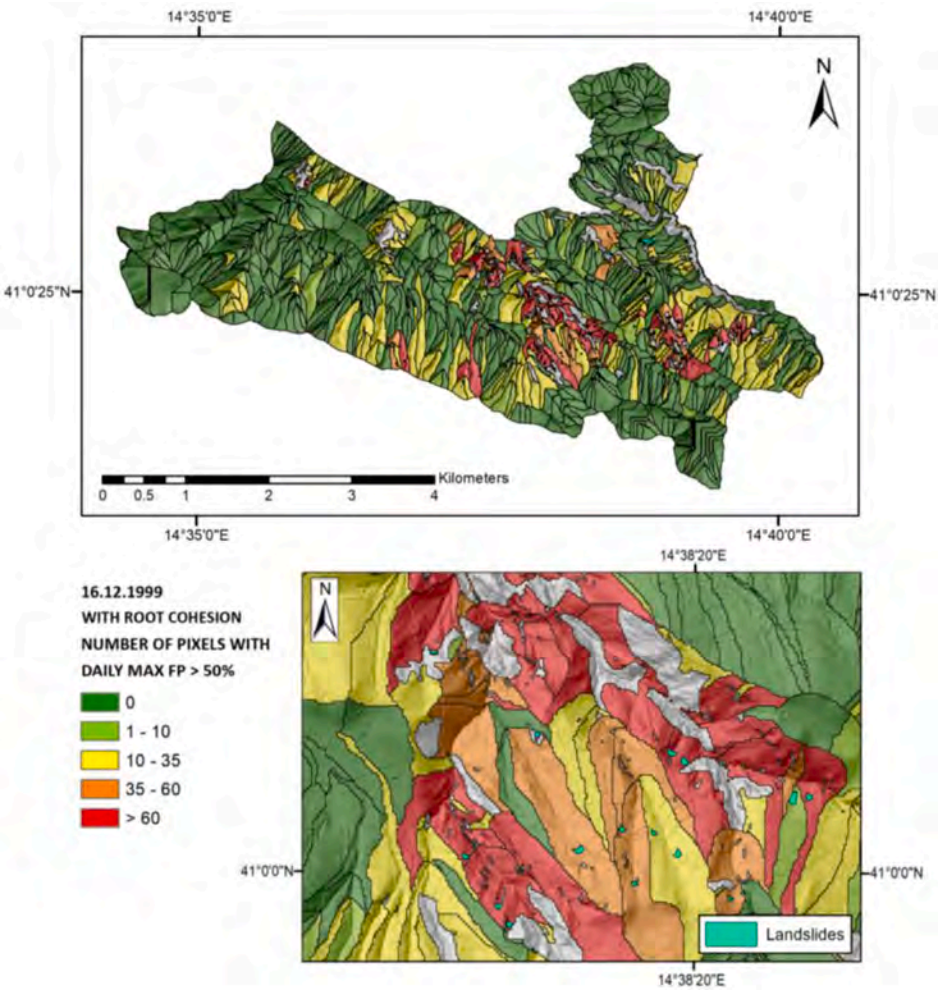

Fig. 18. Cervinara case study, 16.12.1999 simulation with the root cohesion validation: number of pixels with daily max FP higher than 50% of basins and mapped landslides of the event (in cyan). (For interpretation of the references to color in this figure legend, the reader is referred to the web version of this article.)

certain size for instance. The potential criteria to spatially synthesized the data are several, and the choice depends on the context and the purposes for which the simulations are carried out.

For this research, the pixel results of some days of the performed simulations with and without the root cohesion were synthesized into basins through different criteria: mean FP, median FP, number of pixels with the FP higher than a certain threshold (Fig. 17, Fig. 18, Table 8). For each criterium, the obtained maps of the simulations with or without the root cohesion were compared to each other and with respect to the databases of the occurred landslide events.

Table 8
Validation results, where: "RC" is root cohesion; "FP" is failure probability; "FP/pixels number" represents the combination between the thresholds of FP and number of pixels to consider a basin as unstable (i.e. at least × pixels with a FP higher than y); "forecast landslides" is the number of landslides whose perimeter is at least partially overlaid with unstable basins of the model simulation; "TP" is the true positive percentage (correct alarms) i.e. the unstable areas correctly localized by the simulation (the number of unstable basins found by the model with at least one landslide inside it with respect to the actual total unstable basins); "FN" is the false negative percentage (missing alarms) i.e. the unstable areas not localized by the model (the number of the stable basins found by the model with at least one actual landslide inside it with respect to the total actual unstable basins); "TN" is the true negative percentage (correct non-alarms) i.e. the areas correctly defined stable by the model (the basins found stable by the model without landslides inside it compared to the actual total stable basins); "FPS" is the false positive percentage (incorrect alarms) i.e. the areas incorrectly defined stable by the model (unstable basins found by the model without landslides inside it compared to the total actual stable basins).

a)

FP/pixels number	Forecast landslides	TP	FN	TN	FPS
80/1	92,8% (65/70)	68 % (34/50)	32 % (16/50)	89,7% (1519/1693)	10,3% (174/1693)
80/3	88,6% (62/70)	60 % (30/50)	40 % (20/50)	91,6% (1551/1693)	8,4% (142/1693)
60/5	78.6 % (55/70)	54 % (27/50)	46 % (23/50)	94,5 (1600/1693)	5,6% (93/1693)
50/10	85,7% (60/70)	60 % (30/50)	40 % (20/50)	92,2% (1560/1693)	7,8% (133/1693)
45/15	84,3% (59/70)	60 % (30/50)	40 % (20/50)	90,3% (1529/1693)	9,7% (164/1693)
45/25	77,1% (54/70)	50 % (25/50)	50 % (25/50)	92 % (1557/1693)	8 % (136/1693)

b)

FP/pixels number	Forecast landslides	TP	FN	TN	FPS
80/3 without RC	88,6% (62/70)	60% (30/50)	40% (20/50)	91,6% (1550/1693)	8,4% (143/1693)
80/3 with RC	88,6% (62/70)	60% (30/50)	40% (20/50)	91,6% (1551/1693)	8,4% (142/1693)
50/10 without RC	85,7% (60/70)	60% (30/50)	40% (20/50)	92,2% (1560/1693)	7,8% (133/1693)
50/10 with RC	85,7% (60/70)	60% (30/50)	40% (20/50)	92,2% (1560/1693)	7,8% (133/1693)

a) Validation results of the simulation with the root cohesion for different combinations of FP/pixels number; b) Comparison of the validation results between the simulation without the root cohesion and the simulation with the root cohesion.

The differences between the FP basin maps obtained in the simulations with or without the root cohesion were slightly detectable. In Table 8 the results of a comparative validation analysis about the Cervinara case study are presented. The resulting maps of the simulations with and without the root cohesion for the rainy day 16.12.1999 have been elaborated to assess the forecasting capabilities of the model in the two cases. To perform the validation analysis, the pixels FP was aggregated into basins based on thresholds of number of pixels with the FP higher than a certain value. The combination of FP and number of pixels chosen as threshold for the instability and perform the comparative analysis are at least 3 pixels with a FP higher than 80 % and at least 10 pixels with a FP higher than 50 %. Sub-basins resulting exceeding these thresholds were considered unstable and been consequently compared with the landslides locations reported in the database. The landslides database of the 1999 December Cervinara event (AdB-LGV, 2013) reported 70 shallow mass movements of different dimensions, from a minimum of 62 m^2 to a maximum extension of 4400 m^2 and a mean area of 307 m^2, the majority (63/70) of the landslide areas resulted smaller than 500 m^2. Most of the landslides (48/70) was classified as rapid mudflows, 12 as rapid debris flows and 10 as complex movements (rotational slides/flows). All landslides triggered during the event occurred in broad leaved forests, the majority in predominantly holm oak and cork oak forests or predominantly maple, ash, and hornbeam forests.

Other combinations previously explored (with the results of the simulation with the root cohesion only) comparing the basins found beyond the threshold with the distribution of the landslides were 80 %/1 pixel, 60 %/5 pixels, 45 %/15 pixels, 45 %/25 pixels (Cuomo et. al., 2020). All the combinations produced good values of correct alarms and incorrect alarms (Table 8a). The combinations 80 %/3 pixels and 50 %/10 pixels were chosen for the comparative (results with root cohesion vs without root cohesion) validation analysis since considered the best compromises between correct alarms (true positives) and incorrect alarms (false positives) (Table 8a).

The differences between the simulations were so little that the percentages of correct and incorrect alarms resulted the same (with one digit of decimals) in the two cases (Table 8b), confirming what emerged in the previous analyses.

4. Conclusions

The study aimed at overcoming two lacks in the field of the distributed slope stability analyses: a distributed slope stability model capable of a very quick processing in which the root reinforcement is considered; an efficient approach to estimate the root cohesion that it has been tested in large areas and simulating extended periods of rainfall.

The comparative analyses carried out on the results of the simulations performed inserting or not the root reinforcement into the selected model highlighted that the impact of this parameter has been more evident in the outputs of the not rainy days, in terms of failure probabilities of large areas. The finding is attributable to the model adopted to integrate the root cohesion effect into the simulator and to the fact that the simulation outputs were analyzed in terms of failure probabilities and not in terms of pure factor of safety values.

The additional cohesion provided by the root systems integrated into the stability model undoubtedly produced higher values of factor of safety considering the equations on which the stability model is based, and the root cohesion values adopted in the case studies of the research. But concerning the failure probabilities obtained through the Monte Carlo iterations, the root cohesion had a minimal impact on the results, and this behavior was particularly clear when the saturated conditions were reached in the simulations.

The slight differences found in the failure probabilities between the simulations performed inserting or not the root cohesion did not allow to evaluate eventual improvements of the stability model forecasting capabilities validating the results considering actual landslides events. Being indeed the outputs of the simulations with or without the root cohesion quite similar, their validation provided equivalent results.

The research allowed to test a commonly adopted model of the root cohesion by means of applications of a distributed slope stability simulator in regional areas, finding that a different root cohesion model could be preferable in the context of the shallow landslides, in similar areas of the study, and working in terms of failure probabilities. This different model should represent the component of the cohesion due to the presence of the roots in the soil as following a relation of decreasing with the increase of the soil water content different from the relation adopted for the "standard" soil cohesion. In this perspective, further

studies (besides the ones already done) on the relation between the root cohesion and the soil moisture will be extremely useful.

Once found the most appropriate (to our purposes) method to model the root reinforcement, further developments of the research will be addressed to improve the assessing of the vegetation distribution and density using remote sensing techniques and integrating into slope stability HIRESSS other actions (hydrological and mechanical) exerted by the vegetation on the hillslope stability.

Declaration of Competing Interest

The authors declare that they have no known competing financial interests or personal relationships that could have appeared to influence the work reported in this paper.

Data availability

The authors do not have permission to share data.

Acknowledgements

We would like to thank Centro Funzionale Regione Autonoma Valle d'Aosta for the Valle d'Aosta case study and Fabio Matano and Mariagiovanna Moscariello for the Cervinara case study for all the essential discussions held and data provided. We would like to thank Reviewers for time and effort they spent in revisioning, their valuable comments and suggestions helped us in improving the quality of the manuscript.

References

AdB-LGV,2013. Relazione generale sugli studi geologici, geomorfologici, idrogeologici e geotecnici. Accordo di Programma tra Autorità di Bacino dei fiumi Liri-Garigliano e Volturno e Comune di Cervinara, Mitigazione del rischio idrogeologico finalizzato al governo del territorio, Reports B.3.1, B.6.1, B.9.1, pp 124, Caserta, Italy.

Anderson, C.J., Coutts, M.P., Ritchie, R.M., Campbell, D.J., 1989. Root extraction force measurements for Sitka spruce. Forestry: an. Int. J. For. Res. 62 (2), 127–137. https://doi.org/10.1093/forestry/62.2.127.

Arnone, E., Noto, L.V., Lepore, C., Bras, R.L., 2011. Physically-based and distributed approach to analyze rainfall-triggered landslides at watershed scale. Geomorphology 133 (3–4), 121–131. https://doi.org/10.1016/j.geomorph.2011.03.019.

Arnone, E., Caracciolo, D., Noto, L.V., Preti, F., Bras, R.L., 2016. Modeling the hydrological and mechanical effect of roots on shallow landslides. Water Resour. Res. 52 (11), 8590–8612. https://doi.org/10.1002/2015WR018227.

Baum, R.L., Savage, W.Z., Godt, J.W., 2002. TRIGRS—a Fortran program for transient rainfall infiltration and grid-based regional slope-stability analysis. US geological survey open-file report 424, 38.

Bilotta, E., Cascini, L., Foresta, V., Sorbinow, G., 2005. Geotechnical characterisation of pyroclastic soils involved in huge flowslides. Geotech. Geol. Eng. 23 (4), 365–402. https://doi.org/10.1007/s10706-004-1607-3.

Bischetti, G.B., Chiaradia, E.A., Epis, T., Morlotti, E., 2009. Root cohesion of forest species in the Italian Alps. Plant Soil 324 (1–2), 71–89. https://doi.org/10.1007/s11104-009-9941-0-4.

Bistacchi, A., Dal Piaz, G., Massironi, M., Zattin, M., Balestrieri, M., 2001. The Aosta-Ranzola extensional fault system and Oligocene-Present evolution of the Austroalpine-Penninic wedge in the northwestern Alps. Int. J. Earth Sci. 90 (3), 654–667. https://doi.org/10.1007/s005310000178.

Bordoni, M., Meisina, C., Vercesi, A., Bischetti, G.B., Chiaradia, E.A., Vergani, C., Chersich, S., Valentino, R., Bittelli, M., Comolli, R., et al., 2016. Quantifying the contribution of grapevine roots to soil mechanical reinforcement in an area susceptible to shallow landslides. Soil Tillage Res. 163, 195–206.

Bordoni, M., Cislaghi, A., Vercesi, A., Bischetti, G.B., Meisina, C., 2020. Effects of plant roots on soil shear strength and shallow landslide proneness in an area of northern Italian Apennines. Bull. Eng. Geol. Environ. 79, 3361–3381.

Borga, M., Dalla Fontana, G., Gregoretti, C., Marchi, L., 2002. Assessment of shallow landsliding by using a physically based model of hillslope stability. Hydrol. Process. 16 (14), 2833–2851. https://doi.org/10.1002/hyp.1074.

Burylo, M., Hudek, C., Rey, F., 2011. Soil reinforcement by the roots of six dominant species on eroded mountainous marly slopes (Southern Alps, France). Catena 84 (1–2), 70–78. https://doi.org/10.1016/j.catena.2010.09.007.

P, Camerano, P, Terzuolo, P, Varese, I tipi forestali della Valle d'Aosta. Compagnia delle foreste 2007.

Cascini, L., Bonnard, C., Corominas, J., Jibson, R., Montero-Olarte, J., 2005. Landslide hazard and risk zoning for urban planning and development. In: Landslide Risk Management. CRC Press, pp. 209–246.

Cascini, L., Cuomo, S., Guida, D., 2008. Typical source areas of May 1998 flow-like mass movements in the Campania region. Southern Italy. Eng. Geol. 96 (3–4), 107–125. https://doi.org/10.1016/j.enggeo.2007.10.003.

Cascini, L., Cuomo, S., Della Sala, M., 2011. Spatial and temporal occurrence of rainfall-induced shallow landslides of flow type: a case of Sarno-Quindici. Italy. Geomorphology 126 (1–2), 148–158. https://doi.org/10.1016/j.geomorph.2010.10.038.

Chiang, S.H., Chang, K.T., 2011. The potential impact of climate change on typhoon-triggered landslides in Taiwan, 2010–2099. Geomorphology 133 (3–4), 143–151. https://doi.org/10.1016/j.geomorph.2010.12.028.

Chiaradia, E.A., Vergani, C., Bischetti, G.B., 2016. Evaluation of the effects of three European forest types on slope stability by field and probabilistic analyses and their implications for forest management. For. Ecol. Manag. 370, 114–129.

Chok, Y.H., Jaksa, M.B., Kaggwa, W.S., Griffiths, D.V., 2015. Assessing the influence of root reinforcement on slope stability by finite elements. Int. J. Geo-Eng. 6 (1), 1–13. https://doi.org/10.1186/s40703-015-0012-5.

Cislaghi, A., Chiaradia, E.A., Bischetti, G.B., 2017a. Including root reinforcement variability in a probabilistic 3D stability model. Earth Surf. Proc. Land. 42 (12), 1789–1806. https://doi.org/10.1002/esp.4127.

Cislaghi, A., Bordoni, M., Meisina, C., Bischetti, G.B., 2017b. Soil reinforcement provided by the root system of grapevines: Quantification and spatial variability. Ecol. Eng. 109, 169–185.

S, Cuomo, V, Foresta, . Penetration tests in shallow layered unsaturated pyroclastic soil deposits of Southern Italy. In From Fundamentals to Applications in Geotechnics: Proceedings of the 15th Pan-American Conference on Soil Mechanics and Geotechnical Engineering, 15–18 November 2015, Buenos Aires, Argentina 2015 p. 454. IOS Press.

Cuomo, S., Iervolino, A., 2016. Investigating the role of stratigraphy in large-area physically-based analysis of December 1999 Cervinara shallow landslides. J. Mt. Sci. 13 (1), 104–115. https://doi.org/10.1007/s10064-020-01925-5.

Cuomo, S., Masi, E.B., Tofani, V., Moscariello, M., Rossi, G., Matano, F., 2021. Multiseasonal probabilistic slope stability analysis of a large area of unsaturated pyroclastic soils. Landslides 18 (4), 1259–1274. https://doi.org/10.1007/s10346-020-01561-w.

Damiano, E., Olivares, L., Picarelli, L., 2012. Steep-slope monitoring in unsaturated pyroclastic soils. Eng. Geol. 137, 1–12. https://doi.org/10.1016/j.enggeo.2012.03.002.

De Baets, S., Poesen, J., Reubens, B., Wemans, K., De Baerdemaeker, J., Muys, B., 2008. Root tensile strength and root distribution of typical Mediterranean plant species and their contribution to soil shear strength. Plant Soil 305 (1–2), 207–226.

F, Fiorillo, F, Guadagno, Rainfall initiation of debris avalanche-flows in Campania (Italy): a two-phase analysis. In 5th International Conference on Debris-Flow Hazards Mitigation 2011 pp. 53-62.

Fiorillo, F., Wilson, R.C., 2004. Rainfall induced debris flows in pyroclastic deposits, Campania (southern Italy). Eng. Geol. 75 (3–4), 263–289. https://doi.org/10.1016/j.enggeo.2004.06.014.

Fiorillo, F., Guadagno, F., Aquino, S., De Blasio, A., 2001. The December 1999 Cervinara landslides: further debris flows in the pyroclastic deposits of Campania (southern Italy). B. Eng. Geol. Environ. 60 (3), 171–184. https://doi.org/10.1007/s100640000093.

Genet, M., Li, M., Luo, T., Fourcaud, T., Clément-Vidal, A., Stokes, A., 2011. Linking carbon supply to root cell-wall chemistry and mechanics at high altitudes in Abies georgei. Ann. Bot-London 107 (2), 311–320. https://doi.org/10.1093/aob/mcq237.

Giadrossich, F., Guastini, E., Preti, F., Vannocci, P., 2010. Metodologie sperimentali per l'esecuzione di prove di taglio diretto su terre rinforzate con radici. Experimental methodologies for the direct shear tests on soils reinforced by roots. Geol. Tecnica. Ambientale. 4, 5–12.

Gonzalez-Ollauri, A., Mickovski, S.B., 2017. Plant-Best: a novel plant selection tool for slope protection. Ecol. Eng. 106, 154–173.

Gray, D.H., Ohashi, H., 1983. Mechanics of fiber reinforcement in sand. J. Geotech. Eng. 109 (3), 335–353.

Greenway, D.R., 1987. Vegetation and slope stability. In: Anderson, M.G., Richards, K.S. (Eds.), Slope Stability. Wiley, Chichester, pp. 187–230.

Hales, T.C., 2018. Modelling biome-scale root reinforcement and slope stability. Earth Surf. Process. Landf 43, 2157–2166.

Hales, T.C., Miniat, C.F., 2017. Soil moisture causes dynamic adjustments to root reinforcement that reduce slope stability. Earth Surf. Proc. Land 42 (5), 803–813. https://doi.org/10.1002/esp.4039.

Hales, T.C., Cole-Hawthorne, C., Lovell, L., Evans, S.L., 2013. Assessing the accuracy of simple field based root strength measurements. Plant Soil 372 (1–2), 553–565. https://doi.org/10.1007/s11104-013-1765-2.

Hwang, T., Band, L.E., Hales, T.C., Miniat, C.F., Vose, J.M., Bolstad, P.V., Miles, B., Price, K., 2015. Simulating vegetation controls on hurricane-induced shallow landslides with a distributed ecohydrological model. J. Geophys. Res.-Biogeo. 120 (2), 361–378. https://doi.org/10.1002/2014JG002824.

ISPRA, 2018. https://groupware.sinanet.isprambiente.it/uso-copertura-e-consumo-di-suolo/library/copertura-del-suolo/corine-land-cover/corine-land-cover-2012-iv-livello (accessed 13 March 2019).

Iverson, R.M., 2000. Landslide triggering by rain infiltration. Water Resour. Res. 36 (7), 1897–1910. https://doi.org/10.1029/2000WR900090.

Lepore, C., Arnone, E., Noto, L.V., Sivandran, G., Bras, R.L., 2013. Physically based modeling of rainfall-triggered landslides: a case study in the Luquillo forest. Puerto Rico. Hydrol. Earth Syst. Sc. 17 (9), 3371–3387. https://doi.org/10.5194/hess-17-3371-2013, 2013.

Lian, B., Peng, J., Zhan, H., Wang, X., 2019. Mechanical response of root-reinforced loess with various water contents. Soil Till. Res. 193, 85–94. https://doi.org/10.1016/j.still.2019.05.025.

Likitlersuang, S., Takahashi, A., Eab, K.H., 2017. Modeling of root-reinforced soil slope under rainfall condition. Eng. J. 21, 123–132.

Mercalli, L., Berro, D.C., 2016. Cambiamenti climatici e impatti sui territori montani. Scienze del Territorio 4, 44–57.
Montgomery, D.R., Dietrich, W.E., 1994. A physically based model for the topographic control on shallow landsliding. Water Resour. Res. 30 (4), 1153–1171. https://doi.org/10.1029/93WR02979.
Norris, J.E., 2005. Root reinforcement by hawthorn and oak roots on a highway cut-slope in Southern England. Plant Soil 278 (1–2), 43–53. https://doi.org/10.1007/s11104-005-1301-0.
Operstein, V., Frydman, S., 2000. The influence of vegetation on soil strength. Proceedings of the Institution of Civil Engineers-Ground Improvement 4 (2), 81–89.
Pack, R.T., Tarboton, D.G., Goodwin, C.N., 1998. The SINMAP approach to terrain stability mapping Vol. 21, 25.
Pollen, N., 2007. Temporal and spatial variability in root reinforcement of streambanks: accounting for soil shear strength and moisture. Catena 69 (3), 197–205. https://doi.org/10.1016/j.catena.2006.05.004.
N, Pollen, A, Simon, Estimating the mechanical effects of riparian vegetation on streambank stability using a fiber bundle model. Water Resour Res 41:W07025 2005 doi:10.1029/2004WR003801. https://doi.org/10.1029/2004WR003801.
Pollen, N., Simon, A., Collison, A., 2004. Advances in assessing the mechanical and hydrologic effects of riparian vegetation on streambank stability. Riparian vegetation and fluvial geomorphol. 8, 125–139.
F, Preti, F, Giadrossich, Root reinforcement and slope bioengineering stabilization by Spanish Broom (Spartium junceum L.). Hydrol. Earth Syst. Sc., 13 9 2009 1713-1726. https://doi.org/10.5194/hess-13-1713-2009, 2009.
Preti, F., Dani, A., Laio, F., 2010. Root profile assessment by means of hydrological, pedological and above-ground vegetation information for bio-engineering purposes. Ecol. Eng. 36 (3), 305–316. https://doi.org/10.1016/j.ecoleng.2009.07.010.
Preti, F., Schwarz, M., 2006. On root reinforcement modeling. Geophys. Res. Abstr. 8, 4555.
Rhynsburger, D., 1973. Analytic delineation of Thiessen polygons. Geogr. Anal. 5 (2), 133–144. https://doi.org/10.1111/j.1538-4632.1973.tb01003.x.
Roering, J.J., Schmidt, K.M., Stock, J.D., Dietrich, W.E., Montgomery, D.R., 2003. Shallow landsliding, root reinforcement, and the spatial distribution of trees in the Oregon Coast Range. Can. Geotech. J. 40 (2), 237–253. https://doi.org/10.1139/t02-113.
Rossi, G., Catani, F., Leoni, L., Segoni, S., Tofani, V., 2013. HIRESSS: a physically based slope stability simulator for HPC applications. Nat. Hazard Earth Sys. 13 (1), 151–166. https://doi.org/10.5194/nhess-13-151-2013.
Sakals, M.E., Sidle, R.C., 2004. A spatial and temporal model of root cohesion in forest soils. Can. J. Forest Res. 34 (4), 950–958. https://doi.org/10.1139/x03-268.
Salvatici, T., Tofani, V., Rossi, G., D'Ambrosio, M., Stefanelli, C.T., Masi, E.B., Rosi, A., Pazzi, V., Vannocci, P., Petrolo, M., Catani, F., Ratto, S., Stevenin, H., Casagli, N., 2018. Application of a physically based model to forecast shallow landslides at a regional scale. Nat. Hazard Earth Sys. 18 (7), 1919–1935. https://doi.org/10.5194/nhess-18-1919-2018.
Schmidt, K.M., Roering, J.J., Stock, J.D., Dietrich, W.E., Montgomery, D.R., Schaub, T., 2001. The variability of root cohesion as an influence on shallow landslide susceptibility in the Oregon Coast Range. Can. Geotech. J. 38 (5), 995–1024. https://doi.org/10.1139/cgj-38-5-995.
Schwarz, M., Preti, F., Giadrossich, F., Lehmann, P., Or, D., 2010. Quantifying the role of vegetation in slope stability: a case study in Tuscany (Italy). Ecol. Eng. 36, 285–291.
Segoni, S., Rossi, G., Catani, F., 2012. Improving basin scale shallow landslide modelling using reliable soil thickness maps. Natural hazards 61 (1), 85–101.
Simoni, S., Zanotti, F., Bertoldi, G., Rigon, R., 2008. Modelling the probability of occurrence of shallow landslides and channelized debris flows using GEOtop-FS. Hydrol. Process. 22 (4), 532–545. https://doi.org/10.1002/hyp.6886.
A. G. T, Temgoua, N. K, Kokutse, Z, Kavazović, M, Richard, A 3D model applied to analyze the mechanical stability of real-world forested hillslopes prone to landslides. Ecol. Eng., 106, 609-619. https://doi.org/10.1016/j.ecoleng.2017.06.043Tofani, V., Bicocchi, G., Rossi, G., Segoni, S., D'Ambrosio, M., Casagli, N., & Catani, F., 2017. Soil characterization for shallow landslides modeling: a case study in the Northern Apennines (Central Italy). Landslides, 14 2 2017 755-770.
Tosi, M., 2007. Root tensile strength relationships and their slope stability implications of three shrub species in the Northern Apennines (Italy). Geomorphology 87 (4), 268–283. https://doi.org/10.1016/j.geomorph.2006.09.019.
A, Trigila (ed), Rapporto sulle frane in Italia - Il Progetto IFFI: metodologia, risultati e rapporti regionali (Rapporti APAT 78/2007) 2007.
Tron, S., Dani, A., Laio, F., Preti, F., Ridolfi, L., 2014. Mean root depth estimation at landslide slopes. Ecol. Eng. 69, 118–125. https://doi.org/10.1016/j.ecoleng.2014.03.019.
Waldron, L.J., Dakessian, S., 1981. Soil reinforcement by roots: calculation of increased soil shear resistance from root properties. Soil Sci. 132 (6), 427–435.
Wang, X., Hong, M.M., Huang, Z., Zhao, Y.F., Ou, Y.S., Jia, H.X., Li, J., 2019. Biomechanical properties of plant root systems and their ability to stabilize slopes in geohazard-prone regions. Soil Tillage Res. 189, 148–157.
Wu, T.H., 2013. Root reinforcement of soil: Review of analytical models, test results, and applications to design. Can. Geotech. J. 2013 (50), 259–274.
Wu, T.H., McKinnell III, W.P., Swanston, D.N., 1979. Strength of tree roots and landslides on Prince of Wales Island. Alaska. Canadian Geotechnical J. 16 (1), 19–33.
Zydron, T., Skorski, L., 2018. The effect of root reinforcement exemplified by black alder (Alnus glutinosa Gaertn.) and basket willow (salix viminalis) root systems—Case study in Poland. Appl. Ecol. Environ. Res. 16, 407–423.